JOURNAL OF GEOPHYSICAL RESEARCH, VOL. 111, B08408, doi:10.1029/2005JB004083, 2006

Global gravity, bathymetry, and the distribution of submarine volcanism through space and time

A. B. Watts,[1] D. T. Sandwell,[2] W. H. F. Smith,[3] and P. Wessel[4]

Received 1 October 2005; revised 25 April 2006; accepted 4 May 2006; published 31 August 2006.

[1] The seafloor is characterized by numerous seamounts and oceanic islands which are mainly volcanic in origin. Relatively few of these features (<~0.1%), however, have been dated, and so little is known about their tectonic setting. One parameter that is sensitive to whether a seamount formed on, near, or far from a mid-ocean ridge is the elastic thickness, T_e, which is a proxy for the long-term strength of the lithosphere. Most previous studies are based on using the bathymetry to calculate the gravity anomaly for different values of T_e and then comparing the calculated and observed gravity anomaly. The problem with such an approach is that bathymetry data are usually limited to single-beam echo sounder data acquired along a ship track and these data are too sparse to define seamount shape. We therefore use the satellite-derived gravity anomaly to predict the bathymetry for different values of T_e. By comparing the predicted bathymetry to actual shipboard soundings in the vicinity of each locality in the Wessel global seamount database, we have obtained 9758 T_e estimates from a wide range of submarine volcanic features in the Pacific, Indian, and Atlantic oceans. Comparisons where there are previous estimates show that bathymetric prediction is a robust way to estimate T_e and its upper and lower bounds. T_e at sites where there is both a sample and crustal age show considerable scatter, however, and there is no simple relationship between T_e and age. Nevertheless, we are able to tentatively assign a tectonic setting to each T_e estimate. The most striking results are in the Pacific Ocean where a broad swath of "on-ridge" volcanism extends from the Foundation seamounts and Ducie Island/Easter Island ridge in the southeast, across the equator, to the Shatsky and Hess rises in the northwest. Interspersed among the on-ridge volcanism are "flank ridge" and "off-ridge" features. The Indian and Atlantic oceans also show a mix of tectonic settings. Off-ridge volcanism dominates in the eastern North Atlantic and northeast Indian oceans, while flank ridge volcanism dominates the northeastern Indian and western south Atlantic oceans. We have been unable to assign the flank ridge and off-ridge estimates an age, but the on-ridge estimates generally reflect, we believe, the age of the underlying oceanic crust. We estimate the volume of on-ridge volcanism to be $\sim 1.1 \times 10^6$ km^3 which implies a mean seamount addition rate of ~ 0.007 km^3 yr^{-1}. Rates appear to have varied through geological time, reaching their peak during the Late/Early Cretaceous and then declining to the present-day.

Citation: Watts, A. B., D. T. Sandwell, W. H. F. Smith, and P. Wessel (2006), Global gravity, bathymetry, and the distribution of submarine volcanism through space and time, *J. Geophys. Res.*, *111*, B08408, doi:10.1029/2005JB004083.

1. Introduction

[2] The seafloor is characterized by numerous oceanic islands and seamounts, yet little is known about their tectonic setting. There are many age estimates from field mapping on ocean islands, dredging on the flanks of seamounts, and scientific drill sites in guyot tops and nearby moat areas. However, the number of sample ages is small (a few hundred) compared to the total number of seamounts, which by some accounts [*Menard*, 1964] exceed a few hundreds of thousands.

[3] One parameter that may be sensitive to the tectonic setting of a seafloor bathymetric feature is the elastic thickness of the lithosphere, T_e, which is a proxy for its long-term strength. *Watts* [1978] suggested that oceanic T_e depends on the thermal age of the lithosphere at the time of load emplacement and is given approximately by the depth to the 450°C isotherm based on the plate cooling model, a result that has generally been confirmed in subsequent

[1]Department of Earth Sciences, University of Oxford, Oxford, UK.
[2]Scripps Institution of Oceanography, La Jolla, California, USA.
[3]Laboratory for Satellite Altimetry, NOAA, Silver Spring, Maryland, USA.
[4]Department of Geology and Geophysics, School of Ocean and Earth Science and Technology, University of Hawaii, Honolulu, Hawaii, USA.

0148-0227/06/2005JB004083$09.00

papers [e.g., *Caldwell and Turcotte*, 1979; *Calmant et al.*, 1990; *Lago and Cazenave*, 1981; *Wessel*, 1992; *Watts and Zhong*, 2000].

[4] *Watts et al.* [1980] used the dependence of T_e on age to estimate the tectonic setting of ~100 seamounts in the Pacific, a number of which had not been previously sampled. Subsequent studies used T_e to determine tectonic setting not only in the Pacific [*Manea et al.*, 2005], but in the Indian [*Krishna*, 2003] and Atlantic oceans [*Zheng and Arkani-Hamed*, 2002]. However, the total number of such estimates is small compared to the number of seamounts in the world's oceans.

[5] A number of different methods have been used to estimate T_e. These include seismic studies to measure the surfaces of flexure [e.g., *Watts and ten Brink*, 1989] and geomorphic studies of the vertical motions associated with flexure [e.g., *McNutt and Menard*, 1978]. The largest number of estimates, however, has come from forward modeling of the geoid and gravity anomaly. By using a transfer function technique to calculate the anomaly due to the bathymetry and its isostatic compensation and comparing them to the observed anomalies, it has been possible to estimate T_e at a number of oceanic islands and seamounts in each of the world's main ocean basins [*Calmant et al.*, 1990].

[6] The problem with previous gravity modeling approaches is that they have often been applied to ship track sounding data or grids of data that are usually too sparse to fully define the shape of a seamount. As a result, certain assumptions have had to be made in the modeling about the shape of a seamount and whether it is two-dimensional (2-D) or 3-D, which as *Filmer et al.* [1993] have shown may significantly bias T_e.

[7] An alternative approach is to use the global satellite-derived geoid or gravity anomaly, which contains information on the shape of seamounts, to predict the bathymetry for different values of T_e and compare it to observations [e.g., *Goodwillie and Watts*, 1993]. Bathymetric prediction requires, however, implementation of an inverse transfer function. This function grows rapidly at long wavelengths because of isostasy and at short wavelengths because of the attenuation in the geoid or gravity anomaly with increase in water depth. Hence a small error in the gravity anomaly will map into a large error in predicted bathymetry at these wavelengths.

[8] *Dixon et al.* [1983], *Watts et al.* [1985], and *Goodwillie and Watts* [1993] therefore shaped the function in such a way so as to suppress the shortest and longest wavelengths before applying it. By using the geoid derived from satellite altimetry to predict bathymetry they were able to estimate T_e in a range of tectonic settings in the Indian and Pacific oceans.

[9] A different application of the inverse technique is the one by *Smith and Sandwell* [1994a], who used it as a basis to predict bathymetry from satellite gravity anomaly data. They used specially designed filters to shape that part of the inverse transfer function wave band in the range 15–160 km, which was only weakly dependent on T_e. Single ship track echo sounder and multibeam swath bathymetry data were then used to define the bathymetry outside of this wave band.

[10] *Smith and Sandwell* [1994b] extended the prediction wave band so as to calculate bathymetry for different values of T_e. They used a wave band in the range 15–1000 km. This range was sufficiently long to overlap the "diagnostic wave band" of lithospheric flexure, as defined by *Watts* [1983]. By comparing observed and predicted bathymetry in the Atlantic and Pacific oceans south of 30°S (where dense satellite-derived gravity data were then available), they were able to constrain T_e at a number of bathymetric features, including the Louisville Ridge, Walvis Ridge, and Foundation seamounts.

[11] The first detailed application of the inverse technique was the one by *Lyons et al.* [2000] to satellite gravity anomaly data over the Louisville Ridge. They selected the ridge because previous modeling authors [e.g., *Cazenave and Dominh*, 1984; *Watts et al.*, 1988] had made different assumptions about its shape and, as a result, yielded conflicting results. *Lyons et al.* [2000] showed that the inverse technique helped reconcile the previously published results and that T_e was generally low (8–15 km) along the southeastern ridge, south of the Wishbone scarp, and high (23–27 km) to the northwest of it.

[12] The purpose of this paper is to use the global satellite gravity anomaly, together with the inverse transfer function technique of predicting bathymetry, to estimate T_e at selected oceanic islands, seamounts, banks, and rises in each of the world's main ocean basins. Our main aim is to estimate T_e at a greater number of bathymetric features than has been possible in the past and then to use these estimates as a constraint on the distribution of submarine volcanism through space and time.

2. Theory

[13] The gravity anomaly, $G(\mathbf{k})$, associated with seafloor topography, $B(\mathbf{k})$ can be written [e.g., *McKenzie and Bowin*, 1976]

$$G(\mathbf{k}) = Z(k) * B(\mathbf{k})$$

where k is the magnitude of the wave vector $\mathbf{k}$ ($k = (k_x^2 + k_y^2)^{1/2}$), $k = 1/\lambda$, where λ is wavelength, and $Z(k)$ is the transfer function that modifies the topography so as to produce the gravity anomaly.

[14] $Z(k)$ contains information on the state of isostasy and can either be estimated from the free-air gravity anomaly and bathymetry data or calculated for different models of isostasy. For example, $Z(k)$ for the elastic plate (flexure) model of isostasy is given [*Watts*, 2001] by

$$Z(k) = 2\pi G(\rho_c - \rho_w)e^{-kd} \cdot \left\{1 - \Phi(k)\frac{\left((\rho_2 - \rho_i) + (\rho_3 - \rho_2)e^{-kt_2} + (\rho_m - \rho_3)e^{-k(t_2+t_3)}\right)}{(\rho_m - \rho_i)}\right\}$$

where G is gravitational constant, d is mean water depth, ρ_c is density of the seafloor topography, ρ_w is density of seawater, ρ_i is density of the material that infills the flexure, ρ_2 is density of the upper crustal layer, ρ_3 is density of the lower crustal layer, ρ_m is density of the mantle, t_2 is

thickness of upper crustal layer, t_3 is thickness of lower crustal layer, and $\Phi(k)$ is given by

$$\Phi(k) = \left[\frac{Dk^4}{(\rho_m - \rho_i)g} + 1\right]^{-1}$$

where g is acceleration due to gravity and D is flexural rigidity. D is related to the elastic thickness of the plate, T_e, by

$$D = \frac{ET_e^3}{12(1-\nu^2)}$$

where E is Young's modulus and v is Poisson's ratio.

[15] Usually in T_e estimation, the gravity anomaly is computed from the observed bathymetry and compared to the free-air gravity anomaly. T_e is found as the value that best explains the amplitude and wavelength of the gravity anomaly. However, as *Dixon et al.* [1983], *Watts et al.* [1985], *Smith and Sandwell* [1994b], *Lyons et al.* [2000] and *Goodwillie and Watts* [1993] have all demonstrated, T_e may also be estimated by predicting the bathymetry from the gravity (or geoid) anomaly and comparing it to the observed bathymetry. This can be accomplished using

$$B(\mathbf{k}) = Z^{-1}(k) * G(\mathbf{k})$$

where $Z^{-1}(k)$ is the inverse transfer function that modifies the gravity (or geoid) anomaly so as to produce the bathymetry.

[16] Figure 1 shows the functional form of $Z(k)$ and $Z^{-1}(k)$ for $0.001 < k < 0.100$ and a range of assumed T_e, d, and ρ_c values. Other parameters are given in Table 1. Figure 1 shows a strong dependence of $Z(k)$ and $Z^{-1}(k)$ on T_e. $Z(k)$ increases in amplitude and shifts to longer wavelengths as T_e increases while $Z^{-1}(k)$ decreases in amplitude and shifts to longer wavelengths; ρ_c and d have a smaller overall effect and their main influence is on the amplitude of the transfer functions.

[17] $Z(k)$ and $Z^{-1}(k)$ are distinguished by their behavior at long and short wavelengths. $Z(k) \rightarrow 0$ at long wavelengths because of isostatic compensation and at short wavelengths because of upward continuation from the source at the seafloor to the observation point on the sea surface: an effect that increases as $k \rightarrow 1/d$. This behavior causes $Z^{-1}(k)$ to grow rapidly at these wavelengths. Before applying $Z^{-1}(k)$, it is therefore necessary to first shape the function in such a way so as to suppress the longest and shortest wavelengths.

[18] We follow here the "window carpentry" method of *Smith and Sandwell* [1994b, 1997]. They intentionally excluded the diagnostic wave band of flexure: predicting the bathymetry using only the portion of the gravity anomaly spectrum that is shorter than the diagnostic wave band. *Smith and Sandwell* [1994b] chose not to honor actual shipboard soundings, but to use them to calibrate the predictions based on the inverse technique. The reason for this was that they were working with satellite-derived gravity anomaly data south of 30°S where there was little shipboard data. *Smith and Sandwell* [1997] later revised the method to include shipboard data because they were able to obtain more data, better edit the data they had, and extend the coverage to 72°N and 72°S. Thus their bathymetric predictions since 1997 specifically include shipboard data where available.

[19] Our aim in this paper is to estimate T_e by including the flexural wave band that was intentionally excluded by *Smith and Sandwell* [1994b, 1997]. We will determine T_e by minimizing the root-mean-square (RMS) difference between the predicted bathymetry based on different values of T_e and actual shipboard soundings, omitting all locations that have no soundings. In other words, bathymetric predictions including T_e are fit to actual shipboard sounding data, not to predictions that do not include T_e.

[20] We chose two filters for our analysis, $W_1(k)$ and $W_2(k)$. $W_1(k)$ is a high-pass filter designed to reduce $Z^{-1}(k)$ to zero at long wavelengths. *Smith and Sandwell* [1994a] chose $W_1(k)$ to remove the flexure wave band, and so we use here a different $W_1(k)$, with a high and low cut wavelength of 571 and 804 km, respectively, to retain that band. With these values, $W_1(k) = 0.5$ when $k^{-1} = 675$ km. $W_2(k)$ is a low-pass filter designed to reduce $Z^{-1}(k)$ to zero at short wavelengths. *Smith and Sandwell* [1994a] chose a Wiener filter since such a filter is most effective in the high wave number band where there is an exponential growth in $Z^{-1}(k)$ due to water depth. We chose a value of A, the filter constant, of 3900 km^4 which is a smaller than the 9500 km^4 assumed by *Smith and Sandwell* [1994a] because of lower noise levels in the more recent altimeter data [*Sandwell and Smith*, 1997]. With this value, $W_2(k) = 0.5$ when $k^{-1} = 12.5$ km, for water depths of 3 km. The inverse transfer function after it has been modified by the combined filter $W(k) = W_1(k) \times W_2(k)$ is shown in Figure 1 as a solid line in the upper profiles of each panel.

3. Nonlinear Terms

[21] The functions discussed so far are based on a linear admittance theory and so ignore the effect in the expansion of the gravity anomaly of high-order terms in the seafloor topography and its isostatic compensation [*Parker*, 1972]. As a number of workers have pointed out [e.g., *McNutt*, 1979; *Ribe*, 1982; *Smith et al.*, 1989; *Lyons et al.*, 2000], such terms may contribute significantly to the gravity anomaly. *Lyons et al.* [2000], for example, showed that while high-order terms in the topography of the top and bottom of the flexed crust contribute in a negligible way to the gravity anomaly, the contribution to the gravity anomaly of high-order terms in seafloor topography is significant, especially on the crests of tall, steep-sided, low T_e, seamounts where it can exceed 60 mGal.

[22] In order to better understand the effect, we computed the gravity anomaly associated with a synthetic, Gaussian-shaped, seamount in two ways, one using only the first (linear) term ($n = 1$) and the other including higher-order effects. We then used $Z^{-1}(k)$ to estimate T_e from both the linear and higher-order versions of the gravity anomaly. Figures 2a and 2c shows that if $n = 1$ then window carpentry recovers the shape of the input seamount well. However, if $n = 4$ the amplitude of the gravity anomaly increases and the amplitude of the predicted bathymetry exceeds the input bathymetry (Figures 2a and 2b). The effect on the recovery of T_e is shown in Figure 2d. Figure 2 shows that while the

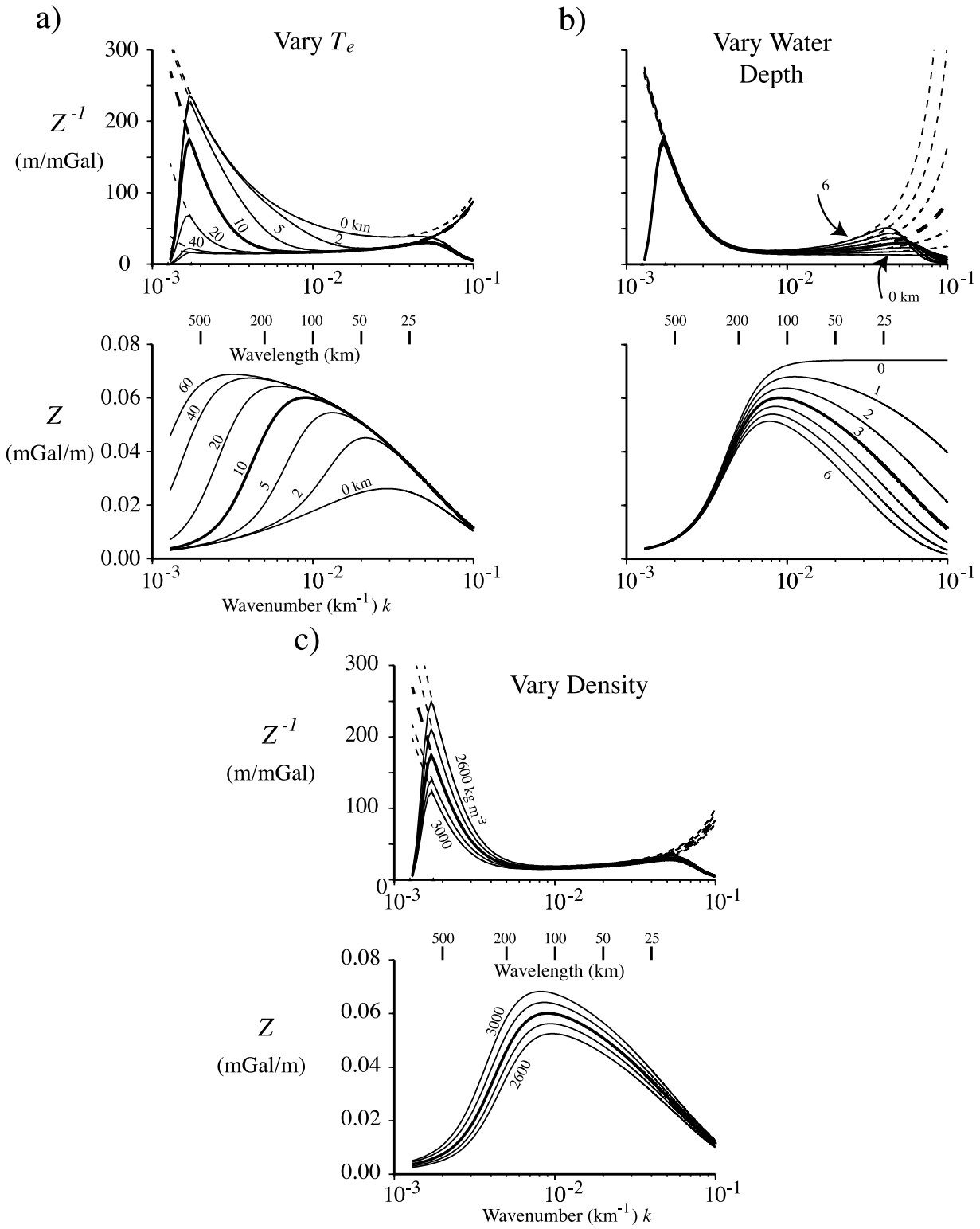

Figure 1. Gravitational admittance for the flexure model of isostasy. The standard model (thick line) is based on an elastic thickness, T_e, of 10 km; water depth, d, of 3 km; and a density of the seafloor topography, ρ_c, of 2800 kg m^{-3}. Other model parameters are as defined in Table 1. Bottom profiles show the admittance, $Z(k)$. Top profiles show the inverse admittance, $Z(k)^{-1}$. The inverse admittance has been tapered at long wavelengths using a cosine filter and at short wavelengths by a Weiner filter [*Smith and Sandwell*, 1994a]. (a) $Z(k)$ and $Z(k)^{-1}$ for a fixed d and ρ_c and T_e in the range 0–60 km. (b) $Z(k)$ and $Z(k)^{-1}$ for a fixed ρ_c and T_e and d in the range 0–6 km. (c) $Z(k)$ and $Z(k)^{-1}$ for a fixed T_e and d and ρ_c in the range 2600–3000 kg m^{-3}.

Table 1. Summary of Parameters Assumed in the Gravity Modeling and Bathymetric Prediction

Parameter	Notation in Equations	Value
Density of seawater	ρ_w	1030 kg m^{-3}
Density of seafloor topography	ρ_c	2800 kg m^{-3}
Density of mantle	ρ_m	3330 kg m^{-3}
Density of oceanic "layer 2"	ρ_2	2800 kg m^{-3}
Density of oceanic "layer 3"	ρ_3	2900 kg m^{-3}
Thickness of oceanic "layer 2"	t_2	1.5 km
Thickness of oceanic "layer 3"	t_3	5 km
Density of material that infills the flexure	ρ_i	2800 kg m^{-3}
Young's modulus	E	100 GPa
Poisson's ratio	ν	0.25
Wavelength of inverse admittance high pass (high cut)		571 km (harmonic degree, 70)
Wavelength of inverse admittance high pass (low cut)		806 km (harmonic degree, 50)

predicted bathymetry for $n = 1$ recovers the input T_e, well, if $n = 4$ a higher T_e is needed in order for the predicted and input bathymetry to match.

[23] These considerations suggest that the linear inverse transfer function technique may overestimate T_e. However, this depends on whether the satellite-derived gravity anomaly field used to predict bathymetry recovers the high-order terms. Closely spaced ship surveys using GPS navigation and modern shipboard gravimeters would be expected to fully recover the gravity anomaly over the crest (and flank)

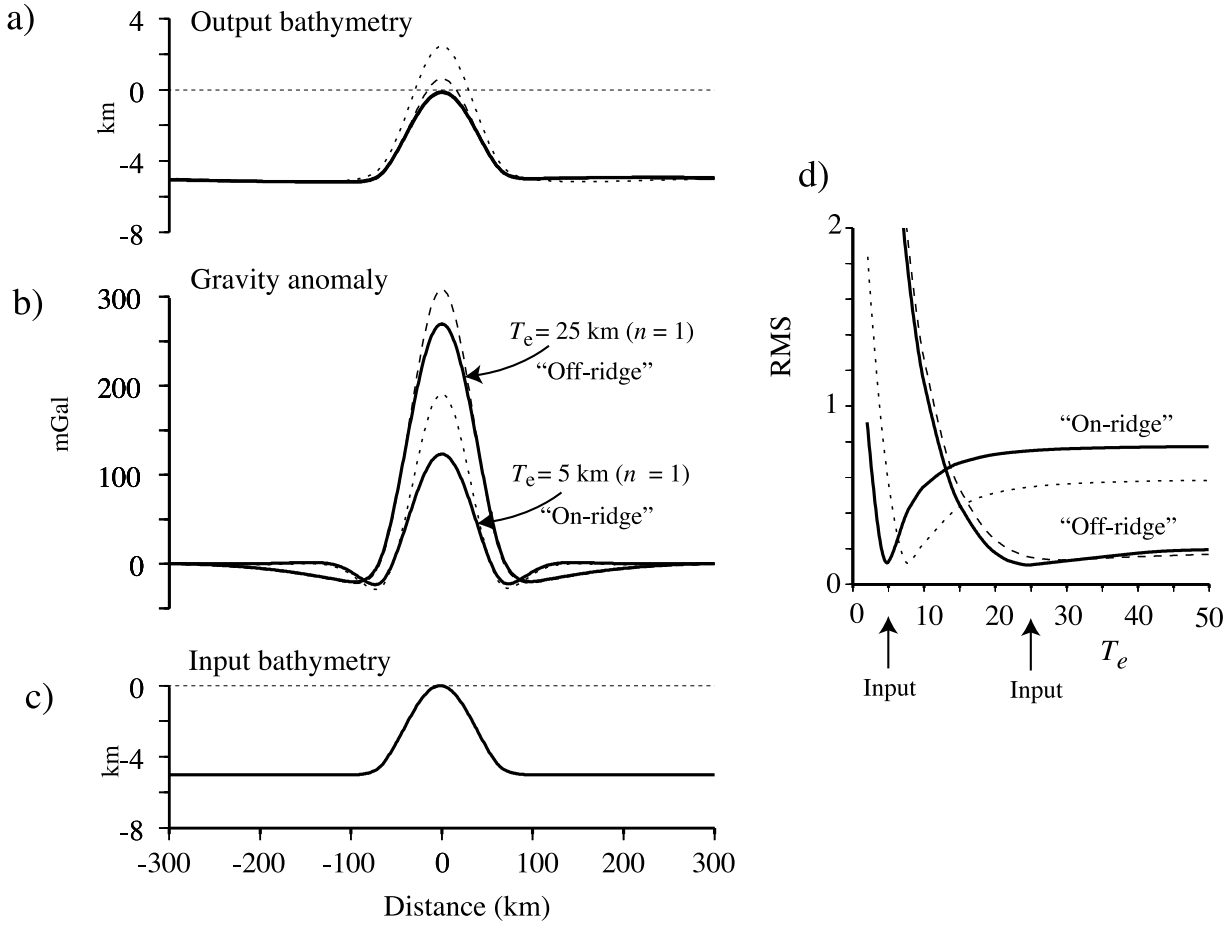

Figure 2. Synthetic tests that use the admittance functions in Figure 1 to calculate the gravity anomaly and predict the bathymetry at a flexurally compensated Gaussian-shaped seamount. (a) "Output" bathymetry based on $Z(k)^{-1}$ and the gravity anomaly in Figure 2b. The output bathymetry for $n = 1$ is the same as the input bathymetry. The output bathymetry for $n = 4$ differs, however, from the input bathymetry. This is because $Z(k)^{-1}$ is based on a linear, first-order, theory. (b) Gravity anomaly based on $T_e = 5$ km (i.e., on ridge) and $T_e = 25$ km (i.e., off ridge) and n in the *Parker* [1972] expansion of 1 (solid lines) and 4 (dashed lines). (c) "Input" bathymetry used to calculate the gravity anomaly. (d) The root-mean-square (RMS) difference between input and output bathymetry for T_e of 5 and 25 km and n of 1 and 4. The effect of the higher-order terms is to overestimate T_e by up to 2.5–5.2 km.

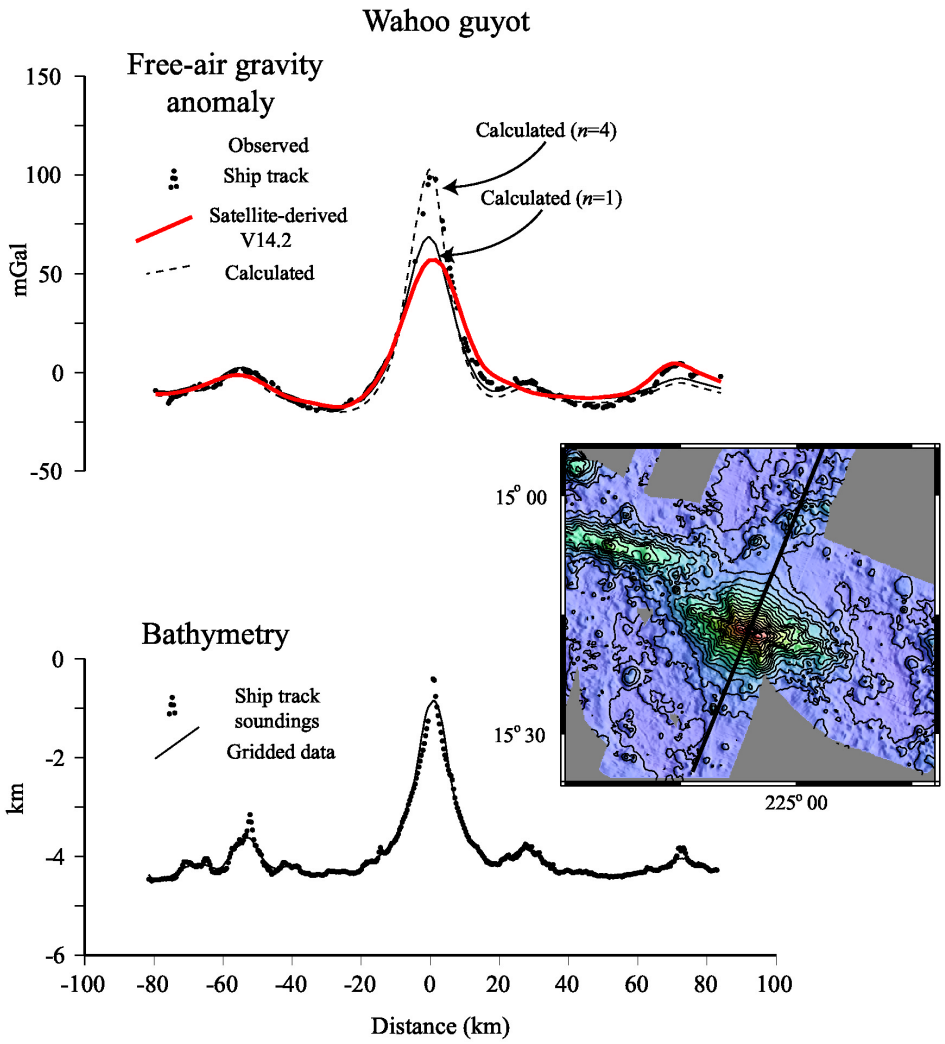

Figure 3. Comparison of the "observed" gravity anomaly recovered from satellite altimeter data to the calculated anomaly based on a grid of shipboard measurements over Wahoo Guyot, Puka Puka Ridge. The inset shows a bathymetry map (contour interval 200 m) based on Figure 3c of *Sandwell et al.* [1995]. (bottom) Shipboard bathymetry measurements (solid circles) and the bathymetry derived from a grid of the measurements (solid line). (top) Observed gravity anomaly based on the satellite-derived V14.2 gravity field of *Sandwell and Smith* [1997] (thick red solid line) and shipboard measurements (solid circles), and the calculated gravity anomaly based on the shipboard grid, T_e = 1.9 km and higher-order terms of 1 (thin solid line) and 4 (dashed line). The calculated gravity anomaly for n = 4 agrees well with the shipboard measurements but poorly with the satellite-derived gravity data. This, in turn, suggests that V14.2 [*Sandwell and Smith*, 1997] may not have sufficient resolution to resolve the higher-order terms.

of a seamount. However, the satellite-derived gravity anomaly is based on altimetry that may not be of sufficient resolution to recover the high-order terms.

[24] That this may be the case is seen at Wahoo guyot (Puka Puka Ridge) in the central Pacific Ocean (Figure 3). The guyot has been extensively surveyed with multibeam bathymetry [*Sandwell et al.*, 1995]. We used the multibeam data to construct a 2 × 2 minute bathymetry grid and then used the grid to calculate the gravity anomaly due to the seafloor topography and its compensation. We assumed a T_e = 1.9 km which is similar to the value estimated by *Goodwillie* [1995]. Figure 3 shows that while the calculated gravity anomaly with n = 1 explains well the amplitude and wavelength of the satellite-derived gravity anomaly it fits poorly the shipboard gravity anomaly data. These data are fit well, however, by the calculated gravity anomaly with n = 4, suggesting that even the most recent satellite-derived gravity fields may not be able to fully recover the higher-order terms.

[25] Wahoo guyot, with its high pedestal height and narrow edifice, is probably a worse case situation as regards the high-order terms. Most other seamounts in the Pacific are smaller and so the contribution to the gravity anomaly of these terms would be expected to be smaller. We have therefore not removed the higher terms in the satellite-

derived gravity field before inverting it for bathymetry as *Lyons et al.* [2000] did, for example, in their study.

4. Method

[26] In their study, *Lyons et al.* [2000] used rectangular 1000 × 1000 km analysis regions centered on the crest of the Louisville Ridge. They estimated T_e in each region from the RMS difference between the observed and predicted bathymetry, selecting the best fit T_e as that value at the RMS minimum. Since we are concerned in this paper with global T_e estimation, we have modified their technique so that it may be used more efficiently.

[27] We first separated the satellite-derived gravity anomaly (V14.2) and the predicted bathymetry (V8.2) grids of *Smith and Sandwell* [1997] into their low-pass and high-pass components using a cosine taper between spherical harmonics 50 and 70, corresponding to wavelengths of 571 and 806 km, respectively. These wavelengths were selected in order to isolate that part of the gravity anomaly and bathymetry spectrum that is dominated by lithospheric flexure from the part that is associated with deep processes, such as those associated with mantle convection.

[28] The main computational steps have been described by *Smith and Sandwell* [1994a, 1997] and so will only be briefly outlined here. The first step is to downward continue the high-pass satellite-derived gravity grid in constant water depth increments of 1 km from 0–6 km. Then, the gravity anomaly at a particular grid cell depth is found from the mean depth (which we estimate from the low-pass predicted bathymetry) and the linear interpolation of the filtered high-pass gravity. The second step is to use the interpolated high-pass gravity, together with the inverse transfer functions, to predict the high-pass bathymetry for different assumed values for the density structure of the crust and T_e. The final step is to sum the low-pass and high-pass predicted bathymetry and compare it to observations based on actual shipboard sounding data.

[29] In order to compare predicted and observed bathymetry at a particular location, we used a cosine "bell" taper, centered at the locality, to define a weighting function and then calculated the RMS difference between the predicted bathymetry based on different assumed values of T_e and the observed bathymetry.

[30] Figure 4 shows an example of the weighting function at two localities in the Line and Hawaiian Islands. We describe the function in terms of a radius, R. With R = 200 km the function has a value of 0.5 at a radius of 100 km. The number of points used in the RMS difference calculation between the predicted and observed bathymetry depends on R, the proximity of the locality to land areas (land areas were excluded), and the available ship track bathymetry coverage. The Line Islands are crossed by relatively few ship tracks and have a small land area while the Hawaiian Islands are crossed by a relatively large number of ship tracks and have a large land area. There is therefore a significantly larger number of comparison points for the locality in the Hawaiian Islands than there is for the Line Islands. Despite this, Figure 4 shows good agreement within both weighted regions (RMS difference between predicted and observed bathymetry of 466.5 m and 467.7 m and correlation coefficient of 0.991 and 0.992 for the Line and Hawaiian islands, respectively). However, the agreement is not perfect. In particular, the predicted bathymetry at the Line Islands locality generally plots below a line with a slope, m, of 1 (i.e., complete agreement between observed and predicted bathymetry) while the predicted bathymetry at the Hawaiian Islands generally plots above it.

[31] The predicted bathymetry shown in Figure 4 is based on an assumed density of the seafloor topography. As was first demonstrated by *Nettleton* [1939] plots of the free-air gravity anomaly against topography should lie on a straight line with a slope that is related to the density of the topography. Plots of the predicted bathymetry (which has been derived from the free-air gravity anomaly) against the observed bathymetry within the weighted region should therefore also lie on a straight line. A slope of m = 1 would indicate a density of seafloor topography of 2800 kg m^{-3}, which is the one assumed in the prediction. Other slopes reflect a different density of the seafloor topography. We can calculate this density from

$$\rho'_c = (\rho_c - \rho_w) * m + \rho_w$$

where ρ_c is the assumed density of the seafloor topography, ρ'_c is the adjusted density, and ρ_w is the density of water. Figure 1 shows that $\rho'_c < \rho_c$ increases $Z^{-1}(k)$ and hence the predicted bathymetry for a particular gravity anomaly while a higher density would decrease it. The adjusted density required at the Line and Hawaiian Islands locality is therefore less (2649 kg m^{-3}) and more (2965 kg m^{-3}), respectively, than the density assumed in the prediction.

[32] Figure 5 shows the RMS difference between predicted and observed bathymetry at the localities in the Line and Hawaiian Islands for different values of R. Both localities show a well-defined RMS difference minimum, although it is better developed in the low T_e Line Islands case than in the high T_e Hawaiian Ridge case. The reason for this is that as T_e increases there is less difference in the flexure and hence a smaller contribution to the gravity anomaly and predicted bathymetry.

[33] We have used the RMS difference minimum, $\mathrm{RMS_{min}}$, to estimate the best fit T_e and the value of $\mathrm{RMS_{min}}$* (1 + x) to estimate its lower and higher bounds, where x is a tolerance parameter. Figure 5 shows that decreasing R sharpens the minimum while increasing R broadens it. T_e decreases with R, but the bias downward is small. The best fit T_e at the Line Islands, for example, decreases from $9.4^{11.6}_{7.4}$ to $6.7^{7.3}_{6.2}$ km (x = 0.05) as R is reduced from 400 to 50 km, respectively (see also Table 2). The choice of R is inevitably a compromise. It should not be so small that only a few points in the region of a volcanic edifice are used or so large that the flexural effects of nearby seamounts are included. We choose in this study R = 200 km, but we consider the effect of a smaller R, especially at those seamounts that are superimposed on rises, such as those associated with the flexural bulge seaward of deep-sea trenches and midplate topographic swells.

[34] Figure 6 compares the RMS difference between predicted and observed bathymetry at the Line and Hawaiian Islands with other localities in the Emperor seamount chain and the Marquesas Islands. We show two

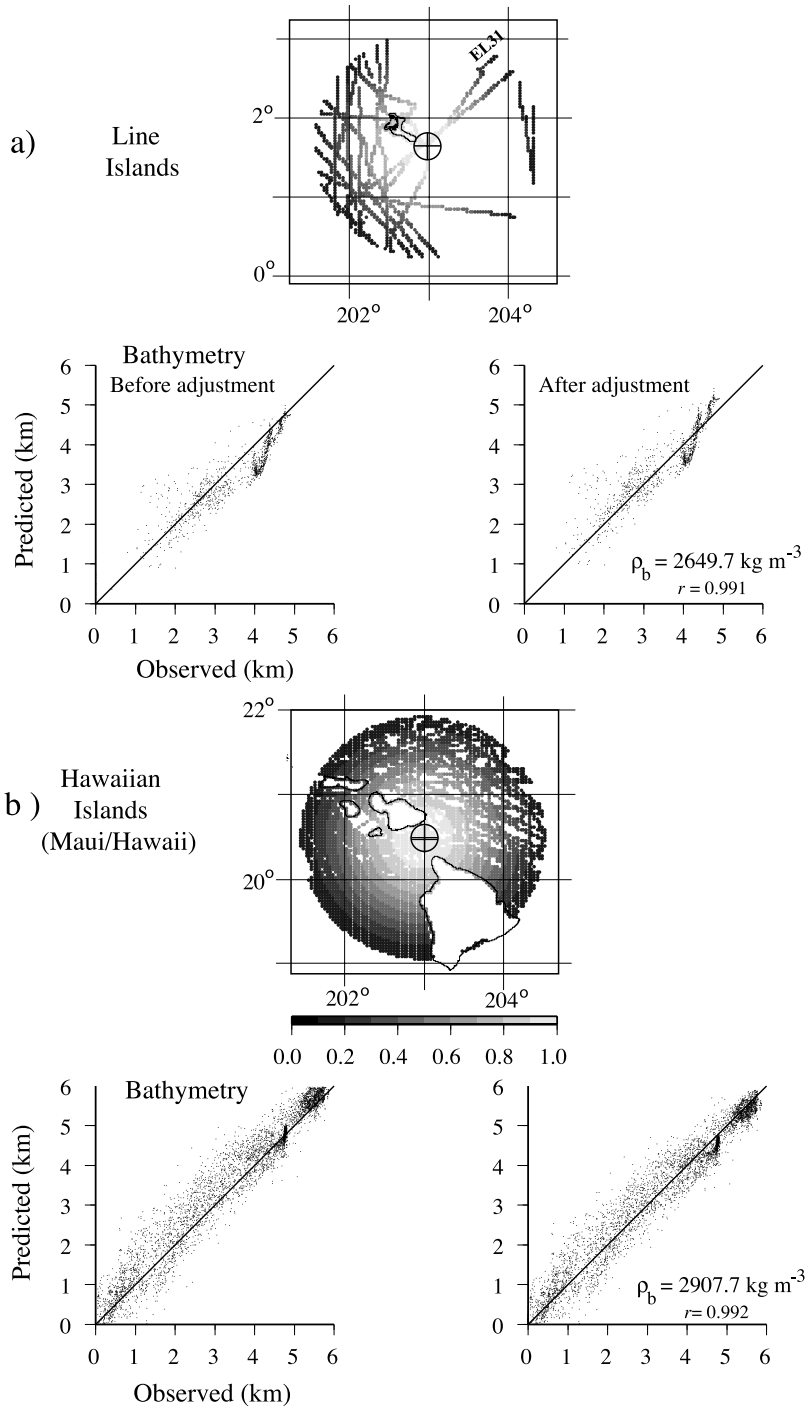

Figure 4. Comparison of observed and predicted bathymetry in a circular region (radius, R, of 200 km) centered on a station (circled cross) in the vicinity of the Hawaiian (longitude 204.0 and latitude 20.5) and Line Islands (longitude 203.0 and latitude 1.6). The observed bathymetry is based on shipboard soundings. The predicted bathymetry has been recovered from the satellite-derived gravity anomaly using the tapered inverse admittance functions in Figure 1 and a T_e that best explains the RMS difference between observed and predicted bathymetry. The thick line in the before adjustment plots shows the expected relationship between the observed and predicted bathymetry if the density of the seafloor topography was 2800 kg m^{-3}. The thick line in the after adjustment plots shows the relationship after adjustment of the seafloor density. (a) Line Islands. (b) Hawaiian Ridge.

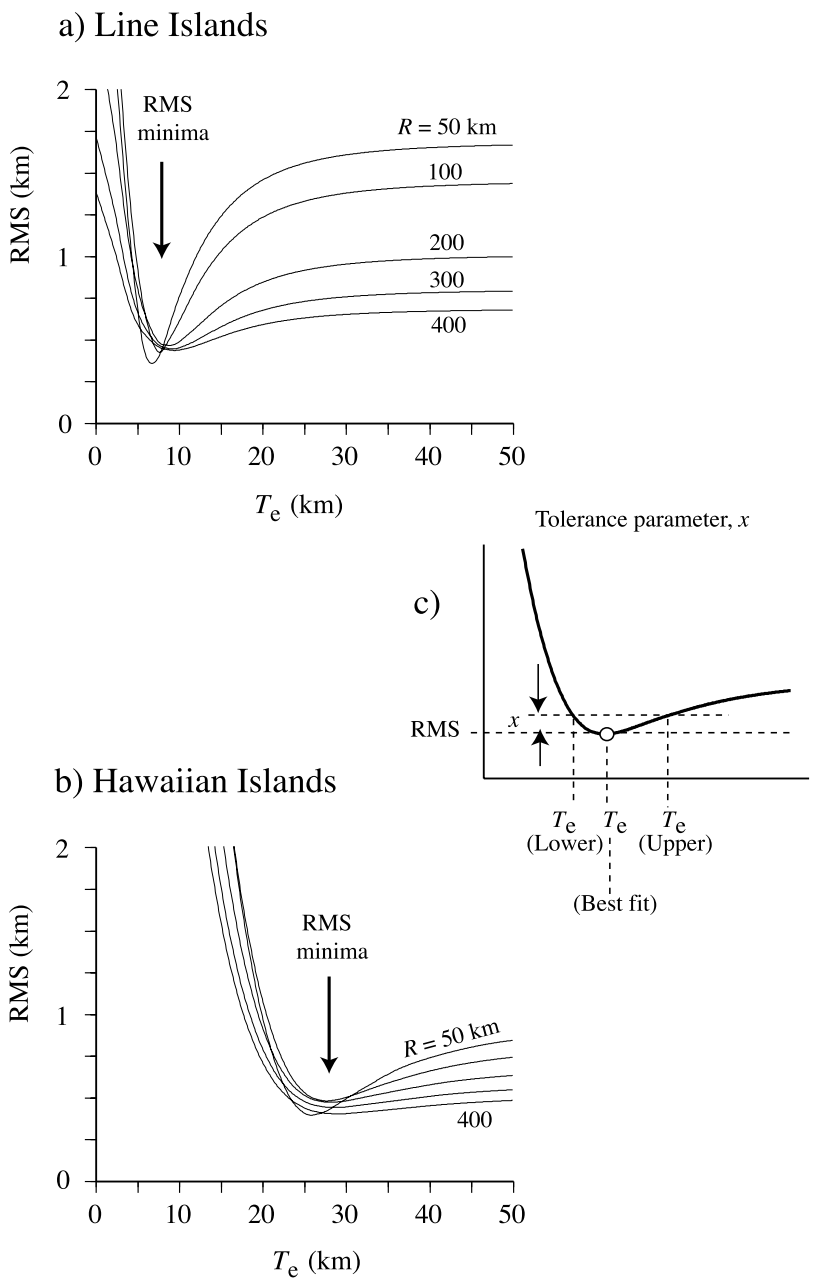

Figure 5. Comparison of the RMS difference between observed and predicted bathymetry for a range of T_e and R values at a station in the region of the (a) Line Islands and (b) Hawaiian Ridge. (c) The best fit and lower and higher bound of T_e. The best fit T_e is defined by the RMS minima. The lower and higher bounds of T_e are defined by the points of intersection where the RMS at the minima has increased by x, the tolerance parameter. The best fit T_e decreases with R. The decrease, assuming $x = 0.05$, is 3.4 km for the Hawaiian Ridge and 2.7 km for the Line Islands.

cases: one where the RMS difference has been computed using a constant density and the other where the density is allowed to vary between the limits 2600 to 3000 kg m^{-3}. Figure 6 shows that while a density adjustment reduces the magnitude of the RMS difference, it also broadens the minimum making it less prominent. The effect on T_e varies with different localities. At the Hawaiian and Line Islands, for example, the best fit T_e is reduced by 0.2 and 1.1 km, respectively, while at the Marquesas Islands and Emperor seamounts it increases by 0.4 and 1.1 km, respectively (see also Table 3).

5. Validation

5.1. Ship Track Data

[35] We first validated the bathymetric prediction technique of recovering T_e using data along ship tracks in the Hawaiian Islands region. This is a well-surveyed area with

Table 2. Dependence of T_e on Radius of the Weighted Points

Longitude	Latitude	Radius, km	Number of Points	Best Fit T_e,[a] km	RMS, m
		Hawaiian Ridge			
204.000	20.500	50	587	$25.8^{27.4}_{24.7}$	390.0
		100	2395	$27.6^{30.2}_{25.6}$	475.4
		200	10495	$27.9^{31.6}_{25.5}$	467.7
		300	21527	$28.8^{33.0}_{25.6}$	436.6
		400	33707	$29.2^{34.1}_{25.7}$	398.0
		Line Islands			
202.981	1.640	50	182	$6.7^{7.3}_{6.2}$	357.9
		100	605	$7.6^{8.1}_{7.1}$	424.2
		200	2341	$8.8^{10.1}_{7.4}$	466.5
		300	5658	$9.2^{10.8}_{7.5}$	444.9
		400	9682	$9.4^{11.6}_{7.4}$	435.8

[a]Best fit T_e together with its lower bound (subscript) and upper bound (superscript). The lower and upper bounds have been computed assuming a tolerance parameter, x, of 0.05.

nearly complete bathymetric coverage so our new inverse approach can be compared with the standard forward approach in which the gravity anomaly is estimated from the bathymetry in order to determine if the two approaches provide consistent estimates of T_e.

[36] Figure 7 shows the calculated gravity anomaly and predicted bathymetry along two ship tracks that intersect the Hawaiian Ridge between Oahu and Molokai. As has been shown previously [*Watts*, 1978], the gravity anomaly in the vicinity of the Hawaiian Islands is a strong function of T_e. This is well seen in Figure 7a which compares the observed free-air gravity anomaly along the ship tracks to calculated gravity anomalies based on the GEBCO 1 minute topographic grid and T_e = 10, 25, and 50 km. (We used the GEBCO grid rather than the predicted topography grid because it is based only on shipboard data). The best fit based on the RMS difference between observed and calculated gravity anomalies is for T_e = 25 km. Figure 7a shows that a lower T_e predicts a gravity anomaly that is of too short wavelength and low amplitude compared to the observed anomaly, while a higher value predicts an anomaly that has too long a wavelength and high amplitude.

[37] Figure 7b shows that the dependence of the calculated gravity anomaly on T_e extends to the predicted bathymetry. The best fit is again for T_e = 25 km. Figure 7b shows that a lower T_e predicts a bathymetry that is of too long wavelength and has too large amplitude compared to the observed, while the higher T_e predicts a bathymetry that is generally of too short wavelength and has too low amplitude. The difference between the best fit T_e and T_e = 50 km is not as large in the predicted bathymetry case, however, as it is in the calculated gravity anomaly case.

[38] Figure 8 compares the predicted bathymetry at Hawaii to the Line Islands, Marquesas Islands, and Emperor seamounts. These features also show a strong dependence of the predicted bathymetry on T_e. This is best seen with reference to the predicted bathymetry for T_e = 16 km (thick solid line). The predicted bathymetry based on this T_e at the Line Islands is too short in wavelength and too low in amplitude compared to the observed suggesting $T_e < 16$ km. The predicted bathymetry based on this T_e at Hawaii, however, has too long a wavelength and too high an amplitude suggesting $T_e > 16$ km. Only at the Emperor seamounts and Marquesas Islands does T_e = 16 km generally account for the observations. These results confirm earlier suggestions that T_e must vary spatially in the Pacific.

5.2. Previous T_e Estimates

[39] During the past three decades, there have been some 25 studies of flexure at oceanic islands and seamounts that have yielded >80 estimates of T_e [see *Watts*, 2001, and references therein]. There is therefore an extensive database with which to compare our estimates based on bathymetric prediction.

[40] Figure 9 compares the T_e from previous estimates with the estimates derived from bathymetric prediction. The previous T_e estimates are based on the work by *Watts* [2001, Table 6.2]. The T_e estimates derived from bathymetric prediction are based on R = 100, 200, and 300 km. We only consider estimates where the difference between the best fit T_e and the lower bound is <15 km. This criterion retains a sharp, well-defined, RMS difference between observed and predicted bathymetry minimum and eliminates broad, poorly defined, minimum. The total number of previous estimates is 94, which reduces to 83 (R = 200 km) and 72 (R = 200 km and adjusted density) after application of the criteria. Horizontal bars on the previous T_e estimates reflect the published uncertainties. Vertical bars on the T_e estimates have been derived from $RMS_{\min}$, assuming x = 0.025. Figure 9 shows generally good agreement

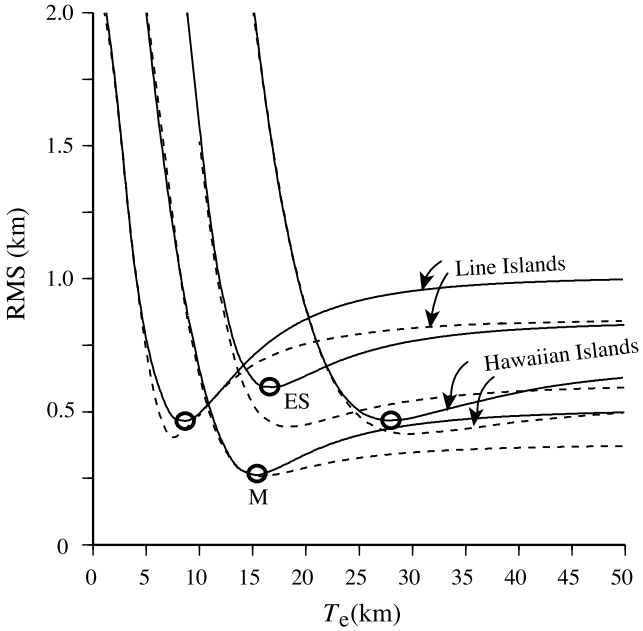

Figure 6. Comparison of the RMS difference between observed and predicted bathymetry for a station in the region of the Line Islands, Emperor Seamounts (ES) (longitude 171.6, latitude 35.0), Marquesas Islands (M) (longitude 220.0, latitude −9.0), and the Hawaiian Ridge. The differences assume R = 200 km and either no adjustment to the density (solid lines) or adjustment (dashed lines). The best fit T_e increases for the Line Islands and decreases for the Marquesas Islands, Emperor Seamounts, and Hawaiian Ridge after application of the density adjustment. The difference (Table 2) is largest for the Hawaiian Ridge (1.8 km) and smallest for the Marquesas Islands (0.4 km).

Table 3. Dependence of T_e on Density Adjustment[a]

	Unadjusted Density				Adjusted Density				
	T_e				T_e				
	Lower	Best Fit	Upper	RMS, m	Lower	Best Fit	Upper	RMS, m	Density kg m^{-3}
Line Islands	7.4	8.8	10.1	466.5	7.0	7.7	8.5	404.1	2689.9
									2649.7
Marquesas Islands	14.1	15.4	16.6	262.6	14.4	15.8	18.0	257.7	2821.1
									2829.8
Emperor Seamounts	15.0	16.9	19.3	593.4	16.4	18.0	21.5	444.6	2974.2
									2988.7
Hawaiian Ridge	25.5	27.9	31.6	467.7	27.0	29.7	35.4	416.2	2890.5
									2907.7

[a] R = 200 km. Bold values indicate the adjusted density of the seafloor topography (e.g., Figure 4).

between the two sets of estimates. This is despite the fact that the previous T_e estimates are based on a wide range of assumptions concerning seamount shape, elastic plate parameters, and the structure of oceanic crust. We found the highest correlation coefficient ($r = 0.63$) is for $R = 200$ km and an adjusted density.

[41] One seamount that has been a focus for new T_e estimation methods is Great Meteor in the central Atlantic Ocean. This seamount has a smooth flat top, rises ~4 km above the surrounding seafloor and is ~150 km across at its base. *Watts et al.* [1975] used an analytical solution of the general flexure equation and ship track gravity data to estimate T_e = 18.9 km which compares with the ~20.0 km estimate of *Verhoef* [1984] and the $19.0^{21.0}_{17.0}$ km estimate of *Calmant et al.* [1990], who used the geoid anomaly derived from Seasat altimeter data and a transfer function technique. More recent estimates have been based on improved geoid data (e.g., GEOSAT, ERS-1) and have yielded estimates of $14.5^{17.0}_{12.0}$ km [*Goodwillie and Watts*, 1993] and 18.2 km and 15.9 km [*Ramillien and Mazzega*, 1999]. These latter estimates compare well to our estimate based on bathymetric prediction of $15.5^{18.1}_{13.4}$ km (R = 200 km). However, Great Meteor is located ~20 km from another Cruiser seamount which as *Verhoef* [1984] demonstrated has a lower T_e than Great Meteor. Therefore a better estimate for the Great Meteor seamount might be one that is based on $R < 200$ km. We found, for example, that T_e increases to $16.0^{21.2}_{14.6}$ km for R = 100 km. Irrespective, the agreement with previous estimates is close, especially when account is taken of the different assumptions that have been made in these studies concerning the elastic parameters, infill density, and density of seafloor topography.

[42] Probably the most direct comparison that we can make between our estimates and previous ones is with those of *Lyons et al.* [2000]. This study used a similar inverse transfer function method and filter design to the one used here. The main differences are that *Lyons et al.* [2000] used satellite-derived gravity V9.2 and predicted bathymetry V6.2 and they calculated the RMS difference between the observed and calculated bathymetry in a rectangular window. Figure 9 and Table 4 show that there is a good agreement between our estimates and those of *Lyons et al.* [2000].

5.3. Seamount Age Data

[43] Previous studies suggest that oceanic T_e depends on the age of the lithosphere at the time of loading [e.g., *Watts and Zhong*, 2000]. Hence there should be some relationship between the T_e estimates derived from bathymetric prediction and age at those localities where there is both a sample age and an age for the underlying oceanic crust.

[44] We therefore constructed a sample age database from the compilations of *McDougall and Duncan* [1988], *Clouard and Bonneville* [2001], *Davis et al.* [2002], *Koppers et al.* [2003], and *Koppers and Staudigel* [2005] in the Pacific Ocean and *O'Connor et al.* [1999] and *Watts* [2001] in the Atlantic and Indian oceans. We then used bathymetric prediction to estimate T_e at each locality in the database, retaining only those estimates that met the RMS difference shape criteria discussed earlier. The number of estimates obtained was 291, the large majority of which (92%) were from the Pacific Ocean.

[45] Figure 10 shows a plot of T_e against age of the oceanic crust at each sample site. Although there is considerable scatter, the data show an upper envelope, which is given approximately by the depth to the 450°C oceanic isotherm, based on the cooling plate model of *Parsons and Sclater* [1977]. The envelope is indicative of a dependence of T_e on age. This is because the T_e of a seamount on oceanic crust of a particular age will be equal or less than that of the youngest seamount: older features will have a lower T_e because they formed on younger lithosphere. A similar reasoning was used by *Wessel* [1997, 2001] to explain scatterplots of the free-air gravity anomaly against age.

[46] Figure 11a shows a plot of T_e against age of the oceanic crust at the time of loading. Again, the plot shows considerable scatter. Many T_e estimates plot outside the expected 300–600°C isotherm range and there is clearly no single controlling isotherm that describes all the T_e data. There is evidence, however, of an increase in the minimum and maximum T_e values over the first approximately 60 Ma and a weak positive correlation (r = 0.36) between T_e and the square root of age.

[47] In an attempt to understand the cause of the scatter in Figure 11a, we have examined the effect on T_e of plate age uncertainties and load-induced stress relaxation. Figure 11b shows all the sample sites, except those from the Cretaceous and Jurassic magnetic quiet zones where the age of the oceanic crust is uncertain. Figure 11c shows all the data, except sites with load ages >50 Ma where significant stress relaxation may have occurred. Figure 11 shows that while r decreases to 0.24 in Figure 11b, it increases to 0.44 in Figure 11c. Therefore uncertainties in magnetic quiet zone age are probably not a major contributing factor to the scatter, but load-induced stress relaxation might be.

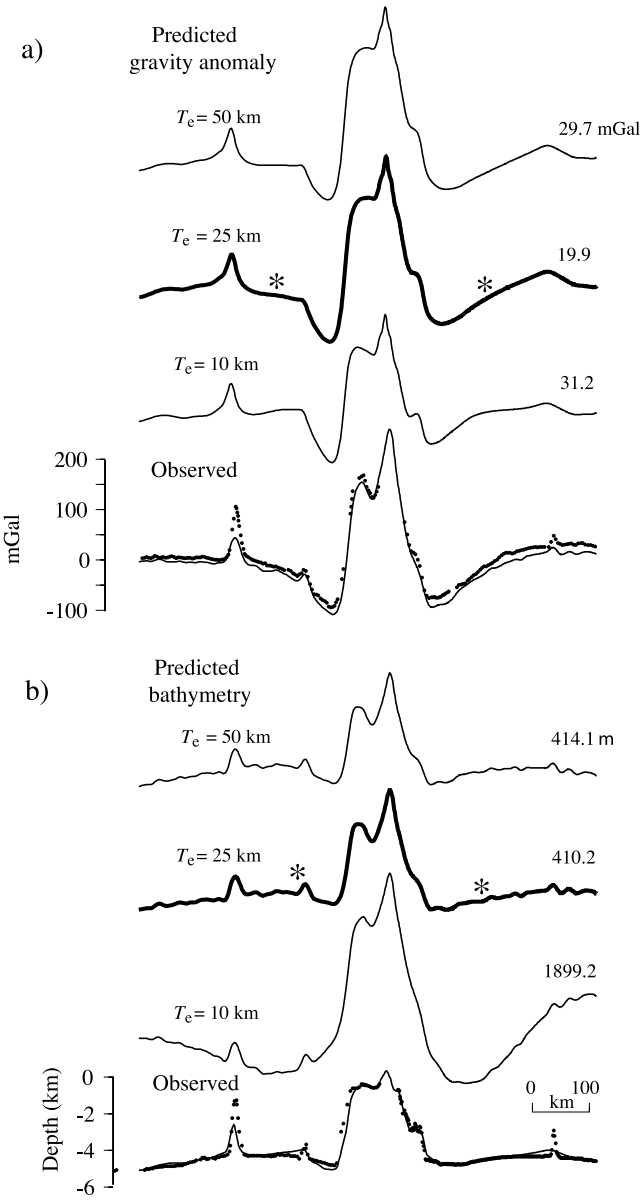

Figure 7. Comparison of observed and calculated gravity anomaly and bathymetry data along a ship track that intersects the Hawaiian Ridge between Oahu and Molokai. The numbers to the right of each profile indicate the RMS difference between observed and calculated gravity and bathymetry data. (a) Observed and calculated gravity anomaly profiles. The observed gravity anomaly data are based on shipboard free-air gravity anomaly data acquired during cruises of V2105 and C1220 (solid circles) and the satellite-derived V14.2 gravity field (solid line). The calculated gravity anomalies are based on a GEBCO 1 minute grid of topography [*British Oceanographic Data Centre*, 2003] and T_e of 10, 25, and 50 km. The asterisks indicate features in the observed data that are particularly well explained by the calculated profiles. (b) Observed and calculated bathymetry profiles. The observed bathymetry is based on shipboard bathymetry data acquired during cruises of V2105 and C1220 (solid circles) and the GEBCO grid (solid line). The calculated bathymetry is based on the inverse admittance functions in Figure 1 and a T_e of 10, 25 and 50 km.

[48] Another possibility are regional variations in, for example, the controlling isotherm. Figures 12a and 12b shows a plot of T_e against age for the Pacific oceanic crust at the time of loading for the *Koppers et al.* [2003], *Davis et al.* [2002], *Koppers and Staudigel* [2005], and *Clouard and Bonneville* [2001] databases. Figure 12 shows that the French Polynesia, Line Islands, Marshall Islands, Gilbert Ridge, and Foundation seamounts (open squares) have a T_e that is lower than the expected 300–600°C isotherm range while the Japanese and Cobb/Kodiak seamounts (open triangles) have a T_e that is higher. T_e at most other sample sites plot within the expected range.

[49] The maps in Figure 12 show the distribution of the sample localities that fall within the expected range, together with the sites that generally have a lower and higher than expected T_e. Sites with low T_e fall in two main regions. The first is French Polynesia and the Foundation seamounts where previous studies [*McNutt and Menard*, 1978; *Calmant*, 1987; *Calmant and Cazenave*, 1987; *Goodwillie and Watts*, 1993; *Clouard et al.*, 2003; *Maia and Arkani-Hamed*, 2002] have already shown that T_e is often smaller than expected. The second is northwest of French Polynesia and includes the Line Islands, Gilbert Ridge, and Marshall Islands. There have, unfortunately, been relatively few previous T_e studies in these regions. However, *Watts et al.* [1980] and *Smith et al.* [1989] also found unusually low T_e at various sites in the Mid-Pacific Mountains and Magellan seamounts. The Magellan seamounts are of interest because they backtrack into the Society Island region of French Polynesia [*Smith et al.*, 1989]. Furthermore, they have some of the same geochemical affinities (e.g., Sr-Nd-Pb isotopic signatures) as the South Pacific Isotopic and Thermal Anomaly (SOPITA) [*Smith et al.*, 1989; *Staudigel et al.*, 1991], as do the Line Islands [*Koppers et al.*, 1998; *Davis et al.*, 2002]. The low T_e sites may therefore reflect the anomalous mantle temperatures associated with the SOPITA that persisted for at least 100 Myr.

[50] In contrast, sites with high T_e are concentrated around the rim of the Pacific (e.g., the Cobb/Kodiak and Japanese seamounts). There are a number of possible explanations for this. One is that our T_e estimates do not reflect the seamounts, but the topographic rise on which they are superimposed. The Cobb/Kodiak and the Japanese seamounts are located, for example, on the flexural bulge seaward of a deep-sea trenches. The width of the bulge is up to 400–600 km and so its associated gravity effect may not have been removed from the high-pass gravity anomaly that was to predict the bathymetry.

[51] That this may be the case is suggested by our T_e estimates at the Cobb/Kodiak seamounts. These seamounts are superimposed on a flexural bulge seaward of the eastern Aleutian deep-sea trench and the Queen Charlotte Trough. Our estimates range from $17.0^{19.9}_{14.8}$ to $27.1^{32.6}_{23.7}$ km (R = 200 km) and are closer to the estimates of *Harris and Chapman* [1994] for the bulge (12–25 km) than they are to their seamount estimates (2–5 km). Indeed, when we assume R = 50 km which focuses the comparison more on the seamounts than the bulge, T_e decreases to $9.9^{15.6}_{8.6}$ to $16.8^{30.6}_{12.7}$ km. These estimates are still not as low as those of *Harris and Chapman* [1994], who used a disc shaped load approximation to the

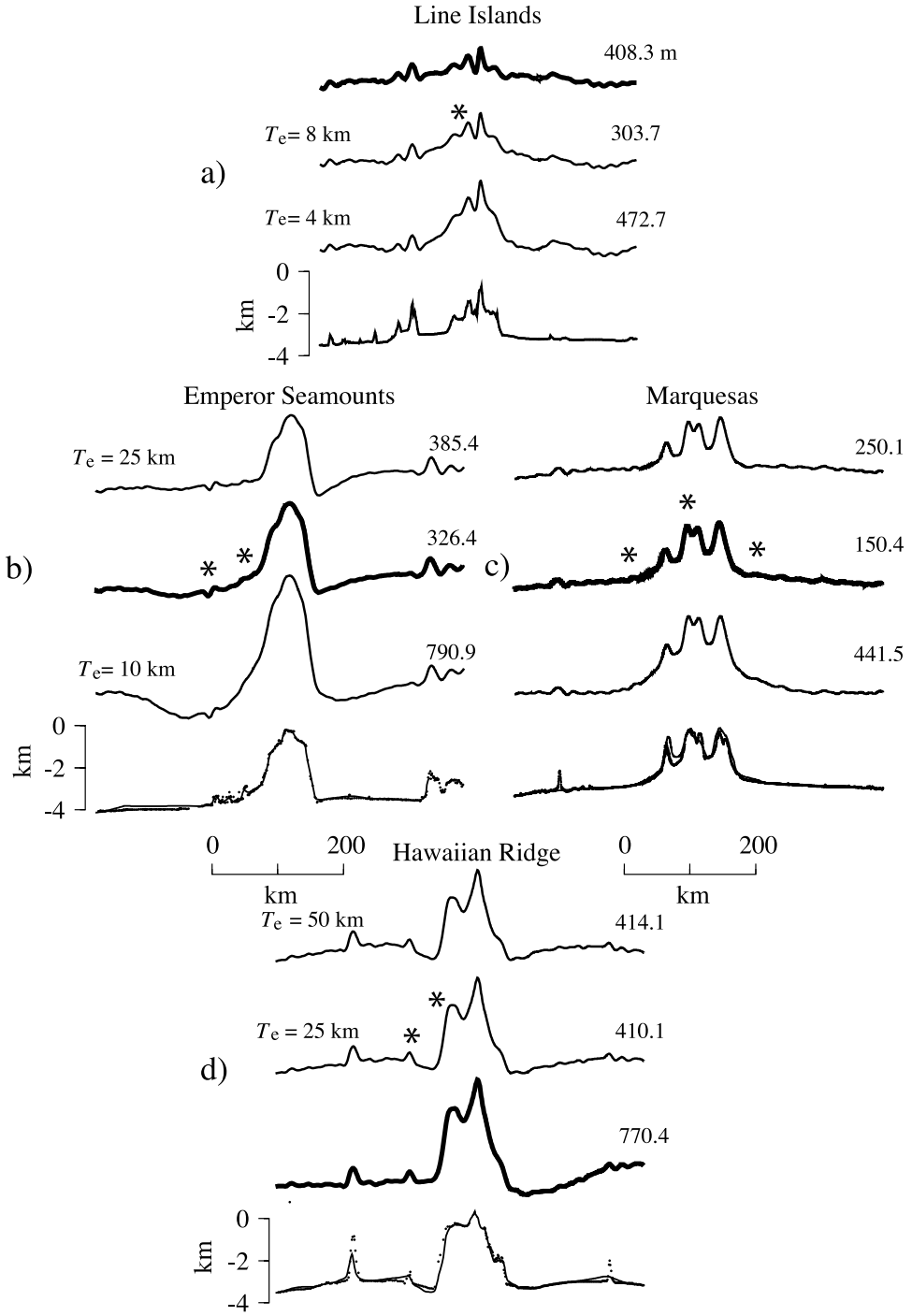

Figure 8. Comparison of observed and calculated bathymetry data along ship track profiles that intersect the Line Islands, Marquesas Islands, Emperor Seamounts, and Hawaiian Ridge. The observed bathymetry (solid circles) is based on data acquired during cruises EL31 (Line Islands), CRGN02 (Marquesas Islands), KK730 and KK750 (Emperor Seamounts) and V2105 and C1220 (Hawaiian Ridge) and the GEBCO grid (thin lines). The calculated bathymetry is based on the tapered inverse admittance functions in Figure 1 and T_e = 10 km (thin line), 8 km (thin line), 16 km (thick line), 25 km (thin line), and 50 km (thick line). (a) Line Islands. (b) Emperor seamounts. (c) Marquesas Islands. (d) Hawaiian Ridge.

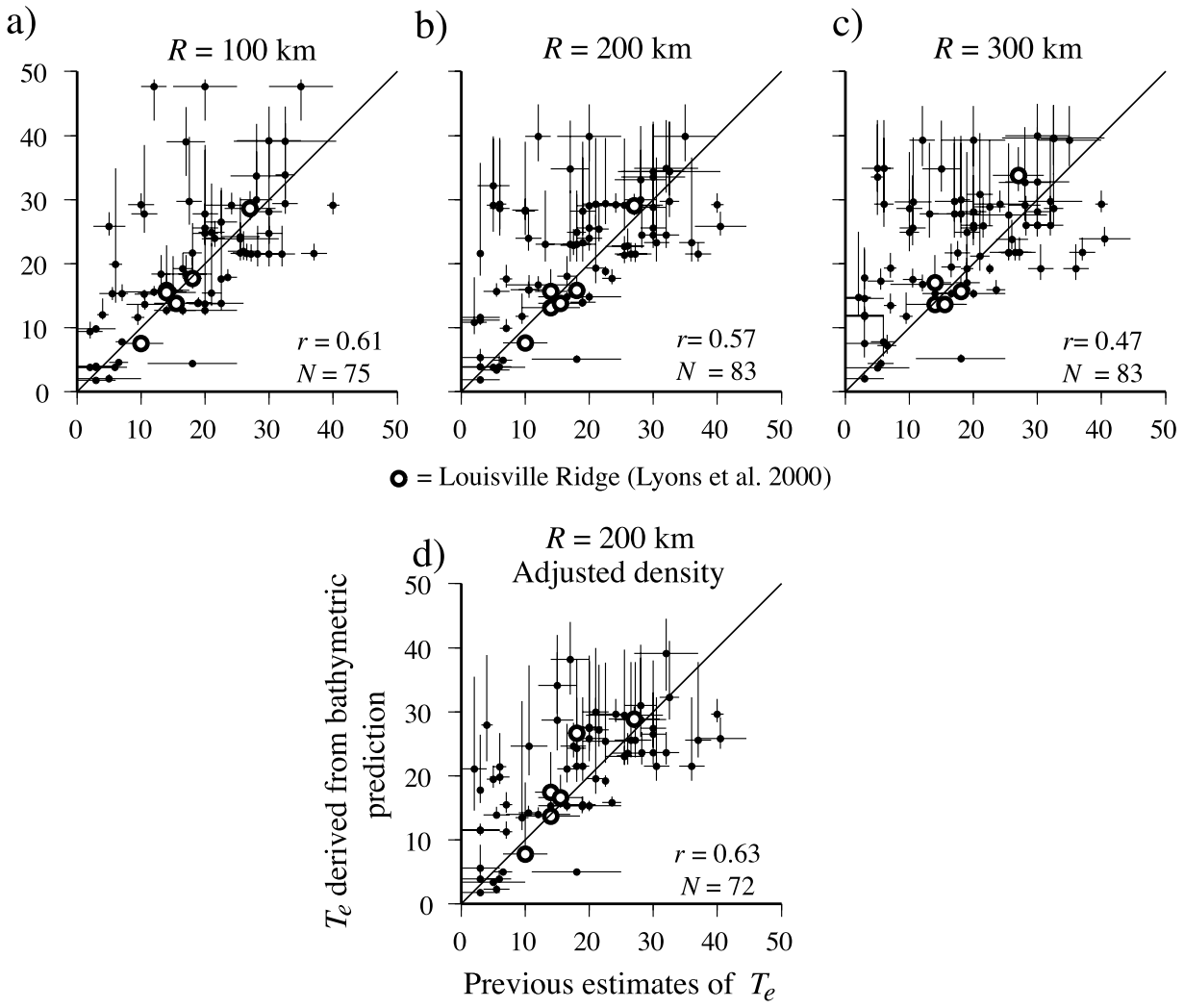

Figure 9. Comparison of previous estimates of T_e to the best fit T_e derived from bathymetric prediction. The previous estimates are based on Table 6.2 of *Watts* [2001]. The "best fit" T_e is shown for different values of R and both unadjusted and adjusted density. (a) R = 100 km and unadjusted density. (b) R = 200 km and unadjusted density. (c) R = 300 km and unadjusted density. (d) R = 200 km and adjusted density. The horizontal bars are based on the observed T_e error range in Table 6.2 of *Watts* [2001]. The vertical bars are based on the lower and higher bounds of T_e and x = 0.025. The open circles compares our estimates of T_e at the Louisville Ridge with those of *Lyons et al.* [2000], who used a similar method to the one used here. N is number of comparison points. The correlation coefficient, r, measures how strong a linear correlation exists between the previous estimate and best fit T_e.

bathymetry in their flexure models, but they are more compatible with a near ridge origin for the seamount chain, as suggested by *Cousens et al.* [1999].

6. Results

[52] We have used the satellite-derived gravity anomaly and shipboard bathymetry measurements to estimate T_e at each locality in the *Wessel* [2001] global seamount database. This database was selected because it contains not only locations, but also size information (i.e., height, base radius) that may be used to estimate the volume of individual seamounts.

[53] The *Wessel* [2001] database yielded a total of 9758 T_e estimates (Figure 13). Not all these estimates are independent since we may have sampled the same bathymetric feature more than once. The average density and T_e of the sampled features is 2810.6 ± 148.5 kg m^{-3} and 18.4 ± 11.0 km, respectively. The symmetry in the lower and upper

Table 4. Comparison of the Results in This Paper With Those of *Lyons et al.* [2000] at the Louisville Ridge

Region of *Lyons et al.* [2000]	Longitude of Center Point	Latitude of Center Point	*Lyons et al.* [2000]	This Paper
A	186.00	−28.00	$27.0_{23.0}^{—}$	$28.9_{25.9}^{32.8}$
F	188.10	−40.70	$15.5_{12.0}^{—}$	$17.4_{13.1}^{30.0}$
G	199.83	−43.00	$14.0_{9.5}^{22.5}$	$13.7_{11.6}^{17.1}$
H	201.80	−45.20	$15.5_{12.0}^{—}$	$16.6_{13.4}^{23.7}$
J	211.80	−47.50	$10.0_{6.5}^{—}$	$7.8_{6.9}^{30.1}$

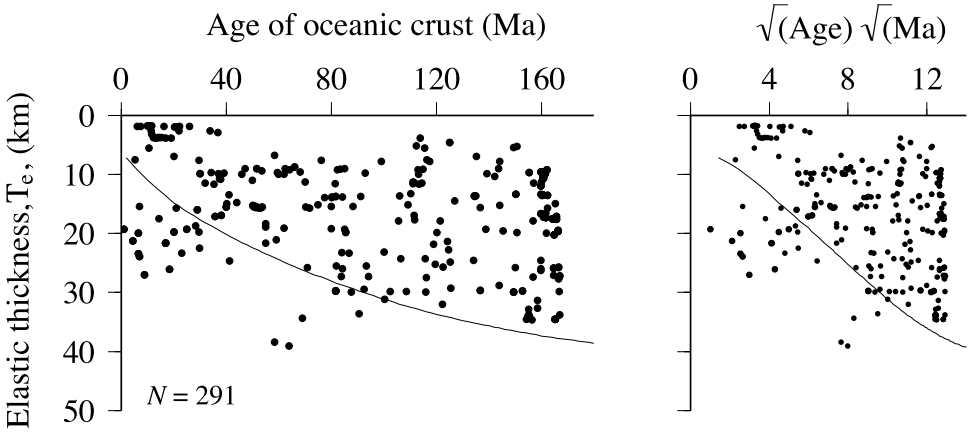

Figure 10. Scatterplot of the best fit T_e derived from bathymetric prediction against age of the oceanic crust at sample sites in the Pacific, Indian, and Atlantic oceans. The best fit T_e is based on $R = 200$ km and an adjusted density. The sample sites are based on the work by *McDougall and Duncan* [1988], *Koppers et al.* [2003], *Davis et al.* [2002], *Koppers and Staudigel* [2005], and *Clouard and Bonneville* [2001] in the Pacific and *O'Connor et al.* [1999] and *Watts* [2001] in the Indian and Atlantic oceans. The age of the oceanic crust is from *Müeller et al.* [1997]. (left) T_e against age of oceanic crust. (right) T_e against the square root of age of oceanic crust. The upper envelope in each plot corresponds approximately to the depth to the 450°C isotherm, based on the plate cooling model of *Parsons and Sclater* [1977]. N is as defined in Figure 9.

bounds (Figure 13b) suggest that the RMS difference between observed and predicted bathymetry is generally well defined and that T_e is well resolved. We attribute this to the high number of bathymetry points (average is 2709.3) used to compute the RMS difference and the relatively low RMS difference (average is 336.9 m) at the minimum.

[54] The remaining 2098 localities in the *Wessel* [2001] database did not yield a T_e estimate. The main reason for this is probably the small size of some of the features. For example, there is a factor of 3 higher proportion of small features (i.e., features with a base radius <8 km and height <1.8 km) among the group that did not yield a T_e estimate than in the rest of the database. A base radius of <8 km corresponds to a wavelength of $<\sim$16 km and most bathymetric features will appear uncompensated and, hence yield no RMS difference minima, at these wavelengths.

[55] Figure 14 shows the global T_e estimates which have been color-coded according to their magnitude. Red dots indicate seamounts where $0 < T_e < 12$ km. This range is similar to that obtained by *Cochran* [1979] and *McNutt* [1979] from spectral studies of seafloor topography at slow spreading and fast spreading ridges in the Atlantic and Pacific oceans and is consistent with the results of more recent studies on intermediate spreading ridges in the Indian Ocean [e.g., *Krishna*, 1997]. We therefore assign seamounts with this T_e range an "on-ridge" setting, although as Figure 11 suggests, "near-ridge" might be a more appropriate description. Blue dots indicate seamounts with $T_e > 20$ km. This lower limit is similar to that obtained by *Watts* [1978] from spectral studies of seafloor topography along the Hawaiian-Emperor seamount chain. We therefore assign such seamounts an off-ridge setting. The remaining (green) dots correspond to intermediate estimates ($12 \leq T_e \leq 20$ km) and so these seamounts are assigned a "flank ridge" setting.

[56] We recognize that such a separation of seamounts into their different settings is arbitrary. This is because each T_e estimate has a lower and higher bound and therefore some estimates may overlap between different tectonic settings. Nevertheless, we believe Figure 14 to be a useful guide. Interestingly, the settings change over small horizontal scales, such that an on-ridge or flank ridge seamount maybe located within a few km of an off-ridge one. Furthermore, the same bathymetric feature (e.g., the Ninetyeast and Chagos Laccadive ridges) may be associated with more than one setting.

[57] The Pacific shows the most striking patterns. Of particular note is a broad swath of on-ridge volcanism that extends for >7000 km from the south central Pacific, across the equator, and into the western Pacific. The swath includes (from southeast to northwest) the Easter/Salas y Gomez ridge, the Ducie Island/Easter ridge, the Foundation Seamounts; the Tuamotu Plateau and Austral Islands; the Line Islands, the Gilbert Ridge and the Mid-Pacific Mountains; and the Shatsky and Hess rises. An on-ridge setting is generally consistent with what is known about the age of these features and the underlying crust. The Easter/Salas y Gomez ridge and Foundation Seamounts, for example, are 0–22 Ma and appear to have been emplaced on 2–10 Myr oceanic crust [*O'Connor et al.*, 1998]. *Maia and Arkani-Hamed* [2002] suggested these features formed at the intersection of the Pacific-Antarctic ridge with a hot spot. The Ducie Island/Easter ridge, which is conjugate to the Easter/Salas y Gomez ridge, probably formed in a similar tectonic setting. There is, however, no clear hot spot age progression along these ridges. It has been proposed that the ridges may have formed by magma leaking either along preexisting lines of weakness [*Bonatti et al.*, 1977; *Searle et al.*, 1995] or subduction-induced tensile cracks [*Sandwell et al.*, 1995]. The Tuamotu Plateau has few sample ages, but *Patriat et al.* [2002] concur with the earlier suggestions of

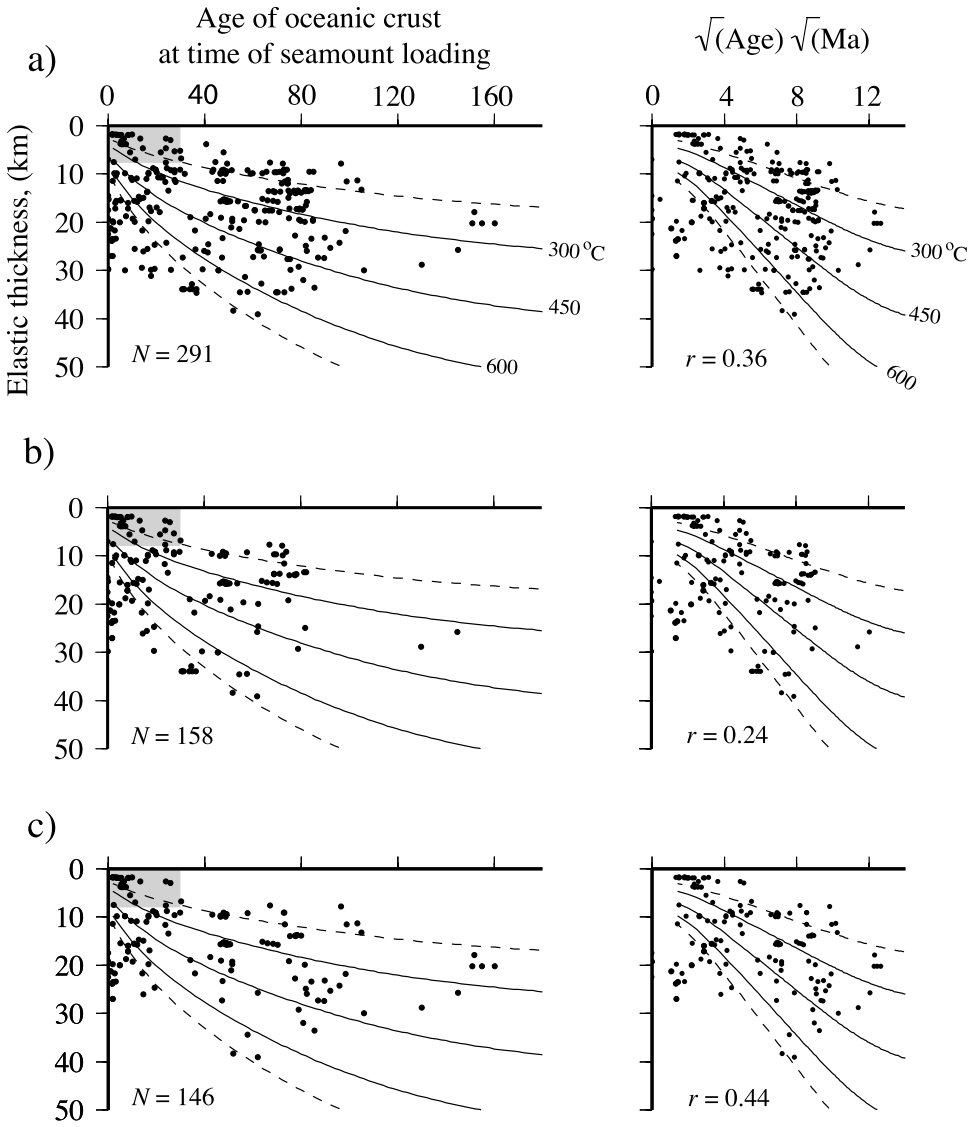

Figure 11. Plot of the best fit T_e derived from bathymetric prediction against age of the oceanic crust at the time of loading at sample sites in the Pacific, Indian, and Atlantic oceans. The sample sites are the same as those used in Figure 10. (left) T_e against age of oceanic crust at the time of loading. (right) T_e against the square root of age of oceanic crust at the time of loading. Thin solid lines show the 300, 450, and 600°C isotherms. Thin dashed lines show the 200°C (uppermost curve) and 700°C (lowermost curve) isotherms. N and r are as defined in Figure 9. Grey shading outlines the region where $0 < T_e < 8$ km and the age of the oceanic crust at the time of loading is 0–30 Ma. (a) All data. (b) All data except sample sites from the Cretaceous and Jurassic magnetic quiet zones. (c) All data except sites where the sample age is >50 Ma.

Watts et al. [1980] that the plateau formed at or near the paleo-East Pacific Rise. The Austral Islands range in age from 3.7 to 39.6 Ma, but most ages cluster in the range 26–32 Ma, suggesting that the bulk of the islands formed on 8–24 Myr seafloor on or near a ridge crest [*McNutt et al.*, 1997]. However, the range of sample ages suggests a less voluminous veneer of volcanism at the Austral islands that may be off ridge [*McNutt et al.*, 1997]. An on-ridge setting is also suggested for the Gilbert Ridge which ranges in age from 64–72 Ma and was emplaced on 63–81 Myr crust [*Koppers and Staudigel*, 2005]. More difficult to reconcile are the Line Islands which range in age from 68 to 86 Ma and so were emplaced on 14–52 Myr oceanic crust [*Davis et al.*, 2002]. These ages are more indicative of a flank ridge, or even off-ridge, tectonic setting than an on-ridge one. One possibility is that the Line Islands, like the Austral Islands, have experienced a prolonged history of volcanism, such that T_e reflects a large-volume early event while the sample ages reflect a small-volume later event. An on-ridge setting for the Shatsky Rise and Hess Rise, however, is in better agreement. The Shatsky Rise ranges in age from 132–146 Ma and formed on or near an Early Cretaceous RRR triple junction [*Sager and Han*, 1993] while the Hess Rise ranges in age from 89–97 Ma and

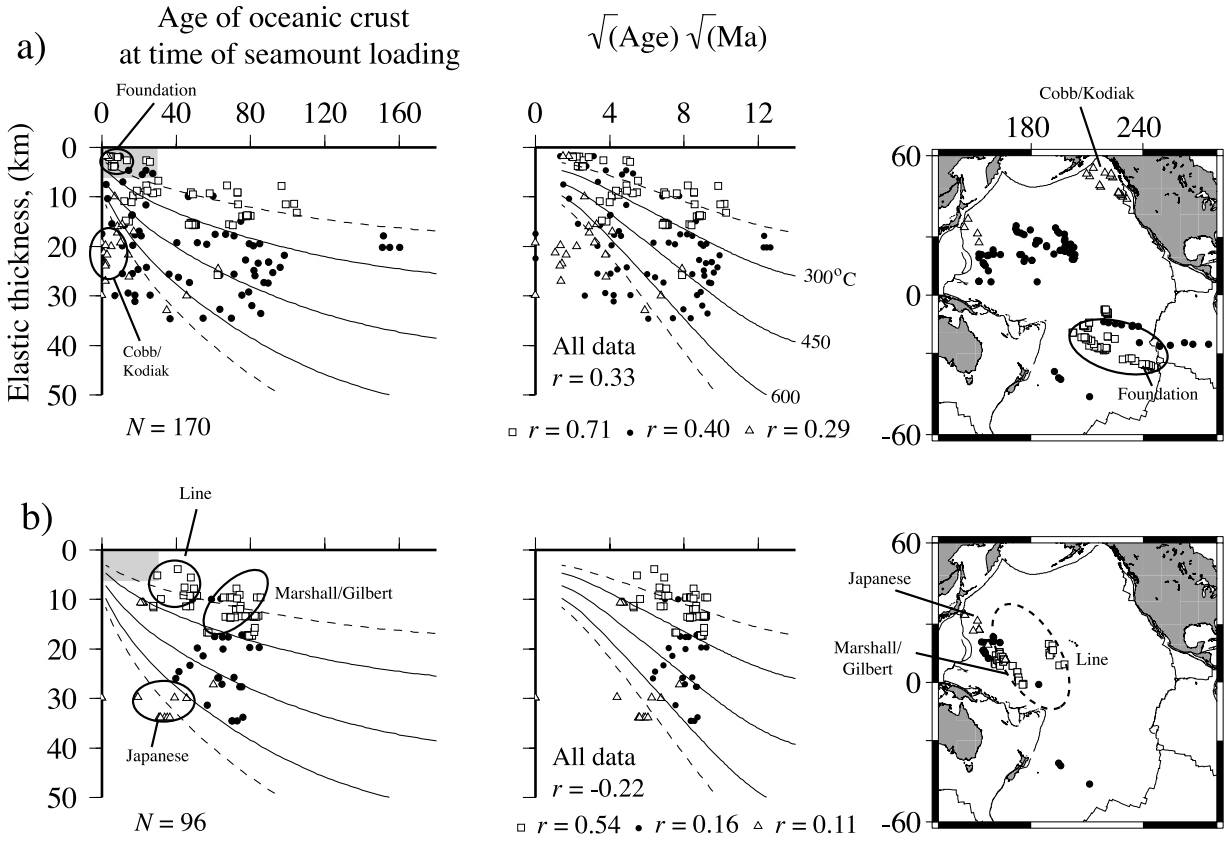

Figure 12. Plot of the best fit T_e derived from bathymetric prediction against age at sample sites in the Pacific Ocean. (left) Plot of T_e against age of the oceanic crust at the time of loading, (middle) plot of T_e against the square root of age of the oceanic crust at the time of loading, and (right) the distribution of the sample sites. Open squares, sites from the French Polynesia, Foundation Seamounts, Marshall/Gilbert Islands, and the Line Islands. Open triangles, sites from the Cobb/Kodiak seamount chain and the Japanese seamounts. Solid circles, all other data. Grey shading, N and r are as defined in Figures 9 and 11. The ellipses show clusters of sample sites where T_e is lower than expected for the 300—600°C isotherm range. (a) *Clouard and Bonneville* [2001] sample sites. (b) *Koppers et al.* [2003], *Davis et al.* [2002], and *Koppers and Staudigel* [2005] sample sites.

formed on or near a Middle Cretaceous R-R-R triple junction [*Clouard and Bonneville*, 2001].

[58] Interspersed among the on-ridge seamounts in the Pacific are off-ridge and flank ridge features (Figure 14). The most prominent off-ridge feature is the Hawaiian Ridge, which ranges in age from ~0–43 Ma and was emplaced on 47–90 Myr oceanic crust [*Clague and Dalrymple*, 1987]. Other off-ridge features are found in the Magellan seamounts and Marcus Wake guyots. The Magellan seamounts range in age from 80 to 100 Ma and were emplaced on 50–70 Myr oceanic crust [*Koppers et al.*, 1998] while the Marcus Wake guyots range in age from 78–126 Ma and were emplaced on 29–77 Myr oceanic crust. These ages are compatible with an off-ridge setting.

[59] The most prominent flank ridge features are the Marquesas Islands, the Cross-Line trend, and the Society Islands. The Marquesas Islands range in age from 1 to 5 Ma and were emplaced on 49–54 Ma oceanic crust. The age of the Cross-Line trend is uncertain, but the late Eocene (36–40 Ma) age of *Schlanger et al.* [1984] suggest they were emplaced on 26–59 Ma oceanic crust. The Cross-Line trend is therefore younger than the Line Islands ridge and so a flank ridge setting is reasonable, given that the Line Islands are mostly on ridge. The Society Islands are 0–4 Ma and were emplaced on 61–85 Myr oceanic crust [*White and Duncan*, 1996] suggestive of an off-ridge rather than a flank ridge setting. However, as *Natland and Winterer* [2005] have pointed out, the Society Islands, like the Marquesas Islands, show some of the same ''cross-grain ridges'' as the Cross-Line trend. The sample ages may therefore reflect small-volume recent volcanism while the T_e reflects a large-volume early event (in this case, late Eocene) along preexisting lines of weakness.

[60] A special feature of the Pacific is that the same geological province may be characterized by one or more settings. For example, the Musician seamounts yield on-ridge and flank ridge settings while the Tasmantid seamounts show flank ridge and off-ridge settings. The Musician seamounts range in age from 82 to 96 Ma and were emplaced on ~0–30 Myr oceanic crust [*Kopp et al.*, 2003] while the Tasmantid seamounts range in age from 6.4 to 24.0 Ma and were emplaced on ~36–64 Myr oceanic crust [*McDougall and Duncan*, 1988]. Both sets of observations are consistent with a mixed setting. Probably the most striking example of a mixed setting is the Mid-Pacific Mountains. Here, off-ridge and particularly flank ridge and

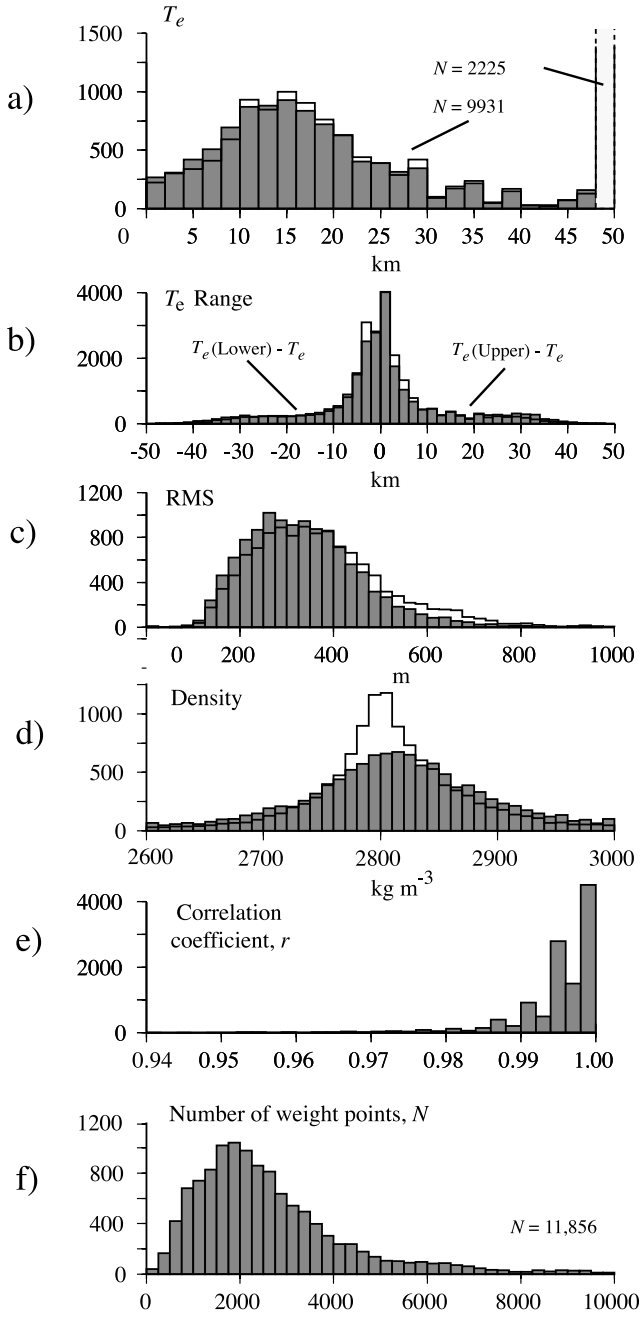

Figure 13. Histograms of parameters derived from bathymetric prediction at all the sites in the *Wessel* [2001] global seamount database. (a) Best fit T_e. (b) High and low bounds of T_e. (c) RMS difference between observed and predicted bathymetry. (d) Density. (e) Correlation coefficient. (f) Number of points used the RMS and correlation coefficient calculations. The stair step lines show the parameters if the density is permitted to vary at each site.

on-ridge settings are juxtaposed. The age of the seafloor in the region is in the range 160–170 Ma which implies volcanism over a long time interval, as indeed appears to have been the case from the few sample ages that are available.

[61] When compared to the Pacific, the Indian Ocean has a small number of T_e estimates. Nevertheless, it shows examples of all three types of tectonic setting. The most prominent on-ridge features are the Ninetyeast and Chagos-Laccadive ridges. The Ninetyeast ridge ranges in age from ~80–38 Ma [*Duncan*, 1991] and is generally considered to have formed when the Kerguelen hot spot was centered on the paleo-Southeast Indian Ridge. The Chagos-Laccadive ridge ranges in age from ~45 to 57 Ma [*Duncan and Hargaves*, 1990] and is believed to have formed when the Reunion hot spot was centered on the paleo-Southwest Indian Ridge. The segmentation of the on-ridge estimates (Figure 14) suggests, however, asymmetry in the thermal properties of the paleo-Indian ridge or, more likely, temporal shifts in the relative location of the ridge crest and hot spot.

[62] Other, more persistent, on-ridge features in the Indian Ocean include the Mascarene Plateau, Madingley Rise, Amsterdam–St. Paul Plateau, Rodriguez Island, Marion Dufresne Rise, and Conrad Rise. The Mascarene Plateau and Madingley Rise are conjugate to the northern part of the Chagos-Laccadive ridge and so together may have formed a large volcanic plateau before seafloor spreading between the Seychelles and western India separated them. The Amsterdam–St. Paul Plateau is located on young seafloor (~10 Ma) at a transform offset of the Southeast Indian Ridge and is historically active [*Johnson et al.*, 2000]. Rodriguez Island is 8–10 Ma and was emplaced on 10–12 Myr oceanic crust, although probably not on a transform. Both sets of ages are therefore consistent with an on-ridge setting. More enigmatic is the on-ridge setting for the Marion Dufresne and Conrad Rise. These features are located south of Crozet Island on 75–90 Ma oceanic crust, but little is known about their age. An on-ridge setting suggests an age that is a little older than the Afansay-Nikitin rise (~80 Ma) which is believed to have formed [*Curry and Munasinghe*, 1991] when the Crozet hot spot was centered on the paleo-Southwest Indian Ridge.

[63] The Indian Ocean is characterized by a number of off-ridge features. Most of these features, however, are located on the crest of the flexural bulge seaward of the Java-Sumatra trench. Christmas Island, for example, is Late Cretaceous to Eocene [*Woodroffe*, 1988] in age and formed on 25–50 Myr oceanic crust [*Exon et al.*, 2002]. We obtained $29.8^{42.4}_{25.7}$ (R = 200 km) for Christmas Island, which is higher than expected based on these age data. When we decreased R to focus more on the island than the bulge, we did not obtain a RMS minimum. However, a nearby seamount (longitude 104.283, latitude −11.517) yielded $28.4^{40.2}_{23.8}$ km (R = 200 km) and $19.1^{21.2}_{16.7}$ km (R = 50 km). This lower value is more compatible with the sample and crustal age data. The Afansay Nikitin seamount is located at the southern terminus of the 85°E ridge [*Curry and Munasinghe*, 1991] and so should not have been influenced by the bulge. According to *Krishna* [2003] the seamount formed during the Late Cretaceous, on ~35 Myr oceanic crust, suggesting a flank ridge rather than an off-ridge setting. We obtained seven T_e estimates at Afansay Nikitin seamount, one of which was flank ridge. Of the remainder, four decreased and two increased when we used a smaller R. The maximum decrease in T_e, however, was only 5–7 km. Our result of a flank ridge setting is therefore robust and suggests that at least part of the seamount and its superimposed rise is younger than Late Cretaceous. More clearly

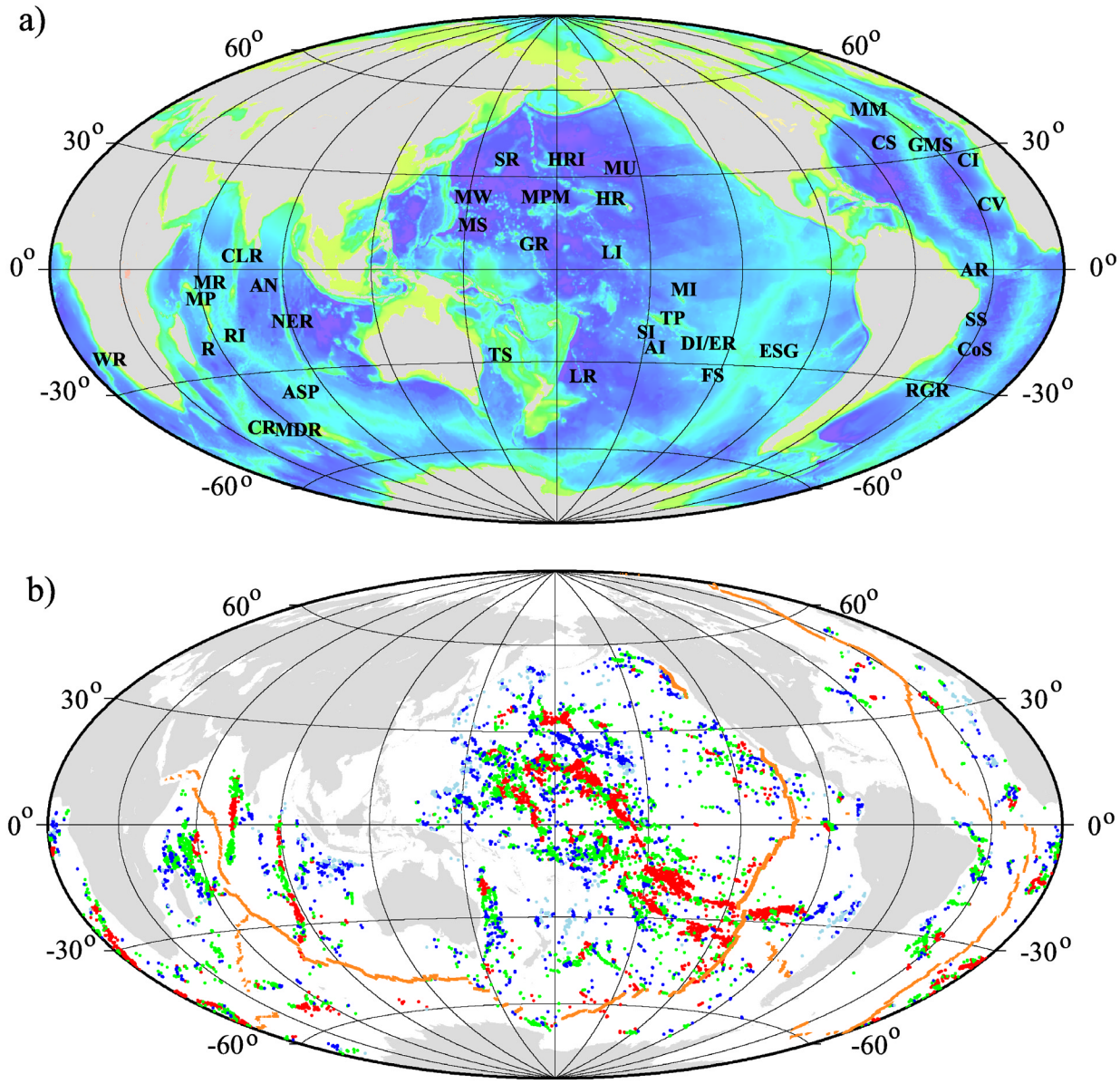

Figure 14. Distribution of on-ridge ($0 < T_e < 12$ km), flank ridge ($12 \leq T_e \leq 20$ km), and off-ridge ($T_e > 20$ km) seamounts in the *Wessel* [2001] global seamount database. (a) Bathymetry map based on the GEBCO 1 min grid showing selected features referred to in the text. AI, Austral Islands; AR, Atol das Rocas seamount; ASP, Amsterdam–St. Paul Plateau; AN, Afansay-Nikitin seamount; CLR, Chagos-Laccodive Ridge; CV, Cape Verde Islands; CI, Canary Islands; CR, Conrad Rise; CS, Cruiser seamount; CoS, Columbia seamounts; DI/ER, Ducie Island–Easter Island ridge; ESG, Easter Island–Salas y Gomez ridge; HR, Hawaiian Islands; HRI, Hess Rise; FS, Foundation Seamounts; GR, Gilbert Ridge; GMS, Great Meteor Seamount; LI, Line Islands; LR, Louisville Ridge; MDR, Marion Dufresne Rise; MPM, Mid-Pacific Mountains; MI, Marquesas Islands; MW, Marcus-Wake Guyots; MR, Madingley Rise; MM, Milne mounds; MP, Mascarene Plateau; MS, Magellan Seamounts; MU, Musician Seamounts; NER, Ninetyeast Ridge; R, Reunion; Rodrigues Island; RGR, Rio Grande Rise; SI, Society Islands; SR, Shatsky Rise; SS, Stocka Seamount; TS, Tasmantid Seamounts; TP, Tuamotu Plateau; WR, Walvis Ridge. (b) Map showing the tectonic setting of seamounts, banks, and rises. Red solid circles, on-ridge. Green solid circles, flank ridge. Blue solid circles, off-ridge. Note that only those estimates where the difference between the best fit and lower bound T_e is <15 km have been plotted. Orange line indicates zero age oceanic crust.

off ridge is Reunion which is <2 Ma [*McDougall*, 1971] and was emplaced on 56–58 Myr oceanic crust [*Charvis et al.*, 1999]. We obtained $34.9^{49.9}_{26.7}$ km at Reunion, consistent with the sample and crustal ages. Also off ridge, although less clearly so, are Mauritius and Crozet Island. Mauritius is 8–10 Ma [*McDougall*, 1971] and was formed on 40–42 Myr oceanic crust while Crozet Island is a Pleistocene shield volcano [*Gunn et al.*, 1970] that was emplaced on 70 Myr oceanic crust. We obtained $20.0^{30.4}_{16.8}$ km and $21.9^{25.9}_{20.0}$ km at Mauritius and Crozet Island, respectively, which is generally consistent with the sample and crustal ages.

[64] A feature of the Indian Ocean is the large number of flank ridge settings. The Nazareth Bank, Seychelles Bank, Maldives/Bombay Ridge, and Chagos Bank in the western Indian Ocean, for example, all yield flank ridge settings. The Seychelles Bank is a granitic ''microcontinent'', but Nazareth Bank (along with the intervening Mascarene Plateau and Saya de Malha Bank) was probably formed during the Eocene/Oligocene by volcanism along the Reunion hot spot track [*Duncan and Hargaves*, 1990]. Therefore the flank ridge setting reflects the movement of the Carlsberg Ridge, which began separating Seychelles and west India ~40 Ma, off the hot spot due to the northward motion of the Indian-Australian plate.

[65] The Atlantic, like the Indian Ocean, is characterized by a mix of settings. In the south Atlantic, most of the seamounts, banks and rises that compose the Walvis Ridge and the northern part of the Rio Grande Rise are on-ridge. These features formed at the intersection of the south Atlantic ridge with a hot spot that is now centered on Tristan da Cunha and Gough Island [*O'Connor and Duncan*, 1990], compatible with an on-ridge setting. Other on-ridge features include the St. Helena seamounts, Discovery seamount, Meteor Rise and the Shona Ridge. The St. Helena seamount chain, like the Rio Grande Rise and Walvis Ridge, probably formed at a hot spot influenced ridge [*O'Connor et al.*, 1999], compatible with an on-ridge origin. The origins of Discovery seamount [*Kempe and Schilling*, 1974], Meteor Rise and the Shona Ridge [*Moreira et al.*, 1995] are unclear, but their close proximity to the R-R-R Bouvet triple junction is consistent with an on-ridge setting. The western South Atlantic is dominated by flank ridge estimates. These include the Columbia, Stocka, Perembuco and Atol das Rocas seamount groups offshore the eastern Brazil continental margin. Unfortunately, few of these features have been dated.

[66] In the North Atlantic, the Cruiser seamounts, the conjugate Corner Rise, and the Milne Mounds are all on ridge. These features are believed to have formed at the interaction of the Mid-Atlantic Ridge with a hot spot that is now centered just to the east of the ridge crest at the Azores [*Gente et al.*, 2003] and so are compatible with an on-ridge setting. The Great Meteor seamount is flank ridge, confirming the earlier suggestion of *Verhoef* [1984] that it formed further from the ridge crest than its immediate neighbor, the Cruiser seamount. The eastern North Atlantic is dominated by off-ridge settings. They include Madeira, Canary, and Cape Verde, all of which are associated with Neogene and younger volcanism [*Carracedo et al.*, 1998; *Stillman et al.*, 1982]. Although there is evidence of older volcanism in both the Canary and Cape Verde islands, most workers consider that the bulk of the islands are <20 Ma and that they were emplaced on old (>120 Myr) oceanic crust, compatible with an off-ridge setting.

7. Discussion

7.1. Distribution of Volcanism Through Space and Time

[67] Previous studies at individual seamounts and oceanic islands [e.g., *Watts*, 1978; *Caldwell and Turcotte*, 1979; *Lago and Cazenave*, 1981; *Calmant et al.*, 1990; *Wessel*, 1992; *Watts and Zhong*, 2000] suggest that T_e is dependent on the age of the oceanic lithosphere at the time of loading and is given approximately by the depth to the 300–600°C oceanic isotherm. Our estimates of T_e at the sample sites where age is known (e.g., Figure 11) suggest, however, that there is no single controlling isotherm that describes all the data. Therefore it may not be possible to use the global T_e data set to estimate age.

[68] We can, however, consider the on-ridge estimates since their age should reflect the age of the underlying oceanic crust. The entire on-ridge database could be used, that is, estimates in the range $0 < T_e < 12$ km. However, Figure 11a suggests that some of these estimates have formed on oceanic crust as old as 100 Ma and therefore maybe more off ridge than on ridge. A better range might therefore be a more limited one. We therefore chose a range of $0 < T_e < 8$ km since Figure 11a shows that a majority of these estimates formed on young oceanic crust, in the range 0–30 Ma.

[69] Figure 15 shows histograms of the age of the on-ridge estimates. Two histograms are shown: one of the entire data set (Figure 15a) and one of a limited data set (Figure 15b). Both histograms show similar patterns. On-ridge volcanism is widely distributed throughout the Cenozoic and Mesozoic. There is a prominent peak at ~90–125 Ma (Albian-Aptian). Other peaks in volcanism occur at ~10 Ma (late Miocene) and ~50 Ma (early Eocene). The timing of the prominent peak is similar to the one deduced by *Wessel* [2001] from free-air gravity anomaly amplitudes and seamount limiting heights.

[70] Figure 15c shows the temporal distribution of the limited on-ridge data set. The solid triangles show on-ridge estimates in time slices of 120–160, 80–120, and 40–80 Ma. The crosses show those sample ages in the *Koppers et al.* [2003], *Davis et al.* [2002], *Koppers and Staudigel* [2005], and *Clouard and Bonneville* [2001] databases that fall within each time slice. Figure 15c shows that on-ridge volcanism was usually accompanied by flank ridge and off-ridge volcanism in the plate interior. The activity was most intense during 80–120 Ma when much of the paleo-East Pacific Ridge crest was active and there was significant off-ridge volcanism as expressed in what now comprises the Magellan, Geologists, Marcus-Wake, and Japanese seamounts.

7.2. Testing the Fixed Hot Spot Hypothesis

[71] There has been much debate recently concerning the fixed hot spot hypothesis and its ability to explain the distribution of submarine volcanism through space and time. The focus of the debate has been on the Pacific Ocean where it has been clear for some time [*Bonatti and Harrison*, 1976; *Epp*, 1984; *Jackson and Shaw*, 1975] that

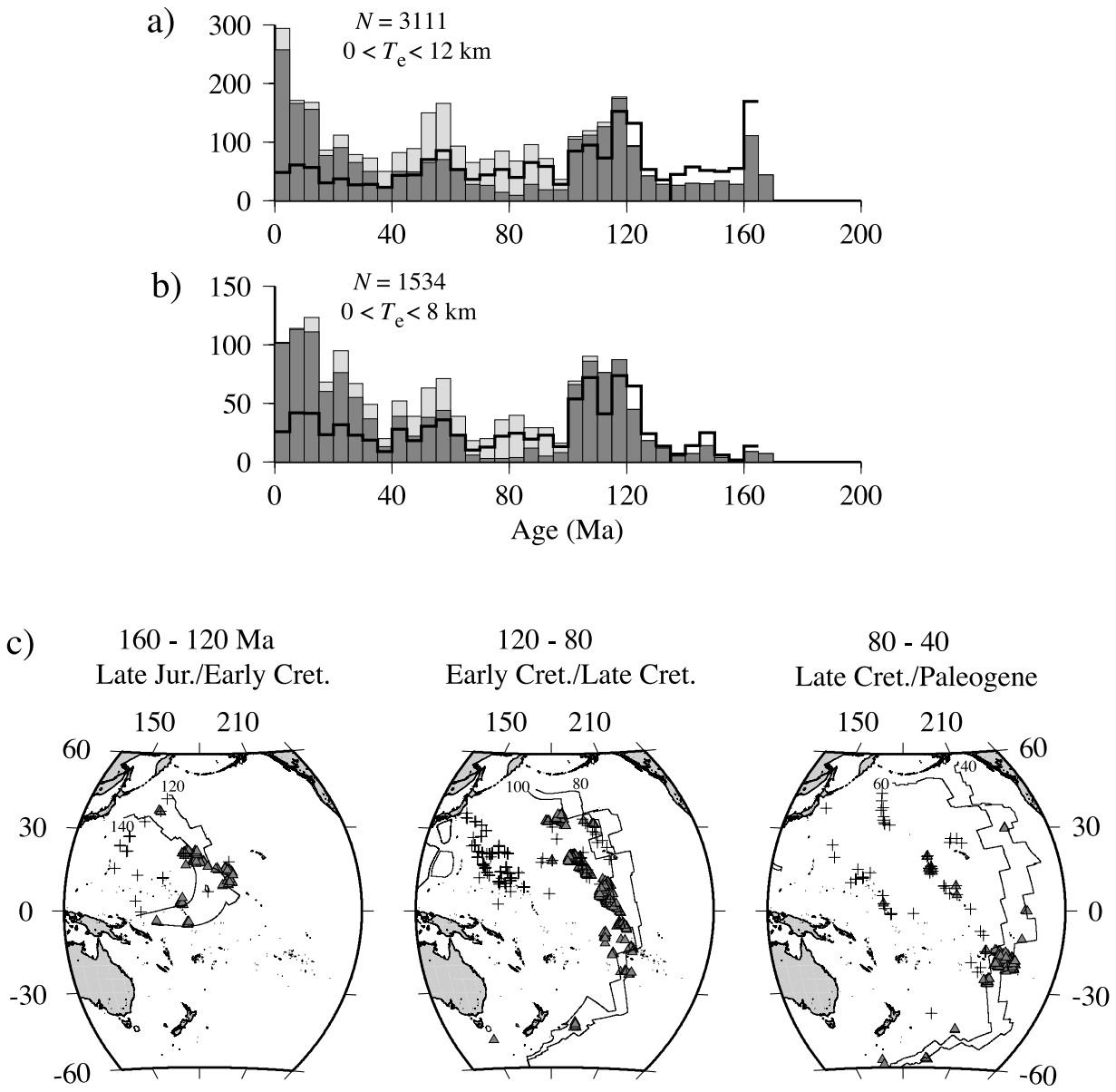

Figure 15. Distribution of on-ridge volcanism through space and time. (a) Histogram of ages based on the estimates where $0 < T_e < 12$ km. *N*, number of estimates. (b) Histogram of ages based on the estimates where $0 < T_e < 8$ km. (c) Maps showing the distribution of volcanism in Figure 15b for three time slices: 160–120 Ma, 120–80 Ma, and 80–40 Ma. Thin lines show selected isochrons (in 20 Myr intervals) based on work by *Müeller et al.* [1997]. Crosses show where samples from the *Clouard and Bonneville* [2001], *Koppers et al.* [2003], and *Davis et al.* [2002] databases have ages that fall within the time slices. Solid triangles show the distribution of the estimates where $0 < T_e < 8$ km that fall within the time slices.

the fixed hot spot hypothesis, while it elegantly explains the progressive increase in age along the Hawaiian Ridge, is unable to explain all the patterns of volcanism that are observed. Since T_e is a proxy for tectonic setting, it may therefore provide an independent way to test the hypothesis.

[72] To examine this further, we have used bathymetric prediction to estimate T_e along the Foundation seamount chain in the south central Pacific. Existing age [*O'Connor et al.*, 1998, 2002], T_e [*Maia and Arkani-Hamed*, 2002], and submarine morphology data are consistent with the formation of these seamounts at a hot spot-influenced paleo-Pacific-Antarctica ridge crest. If this is correct, then the younger eastern end of the chain should have formed on young seafloor while the older western end should have formed on old seafloor.

[73] Figure 16 compares the estimated T_e based on bathymetric prediction to the expected T_e based on the fixed hot spot hypothesis. Figure 16 shows a plot of the estimated and expected T_e against distance from the inferred position of the hot spot that generated the Foundation seamount chain. T_e has been estimated at each seamount digitized from the predicted bathymetry maps of *Smith and Sandwell* [1994a] by *Koppers et al.* [2001]. We show the RMS difference between observed and predicted bathymetry at

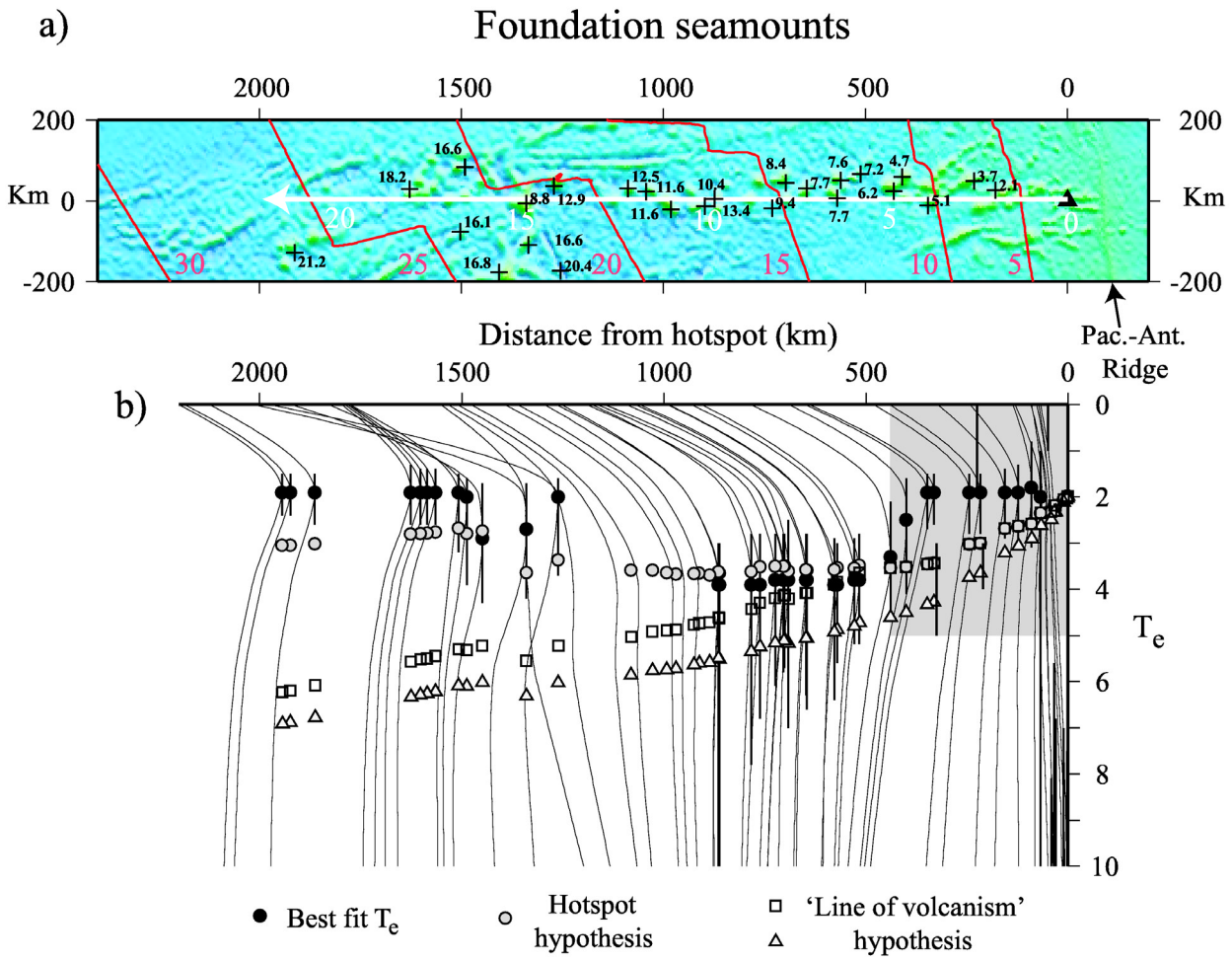

Figure 16. Test of the fixed hot spot hypothesis at the Foundation seamount chain. (a) Predicted bathymetry projected into the frame of the Hawaiian stage pole between 43 and 0 Ma (longitude 294.67, latitude 67.01). The white arrow and white numbers show the predicted age progression in Myr of the Foundation Seamounts for a hot spot located at longitude 248.25, latitude −37.32, just to the west of the Pacific-Antarctica ridge crest. Crosses and bold numbers show radiometric age dates based on *O'Connor et al.* [2002]. (b) RMS difference between observed and predicted bathymetry plotted as a function of distance from the hot spot. Solid circles show the best fit T_e and vertical bars show upper and lower bounds. Gray circles show the expected T_e based on the fixed hot spot hypothesis and a 200°C controlling oceanic isotherm. Open squares and triangles show the expected T_e based on the "line of volcanism" hypothesis. Triangles assume that the entire seamount chain was emplaced on the seafloor today. Squares assume that the first 5 Myr formed according to the hot spot hypothesis and then >5 Ma was formed according to the line of volcanism hot spot hypothesis. The gray shaded region shows the region of the *Maia and Arkani-Hamed* [2002] study whose T_e estimates in the first 5 Myr along the chain (0–5 km) are in general accord with our results.

each seamount, together with the best fit T_e and its lower and upper bounds. The expected T_e is based on a controlling isotherm of 200°C which is lower than normally assumed in flexure studies. However, it is the same controlling isotherm as was deduced by *Maia and Arkani-Hamed* [2002] at the young (<5 Ma) end of the chain. The distance has been computed by projection along a small circle about the Hawaiian stage pole (latitude 67.017, longitude 294.467). Figure 16 shows that the expected T_e should increase away from the Pacific-Antarctica ridge crest as the age difference between the age of the seamount and the underlying oceanic crust increases, and then decreases as the seamounts cross from the older to the younger side of an unnamed fracture zone between the Resolution and Mocha fracture zones [*Maia and Arkani-Hamed*, 2002]. This pattern in the expected T_e is repeated in the estimated T_e. We conclude therefore that our estimates of T_e derived from bathymetric prediction are in accord with the hot spot hypothesis, at least along the Foundation seamount chain.

[74] Of interest is to determine whether it might be possible to use our T_e estimates to resolve between the hot spot hypothesis and the competing "line of volcanism"

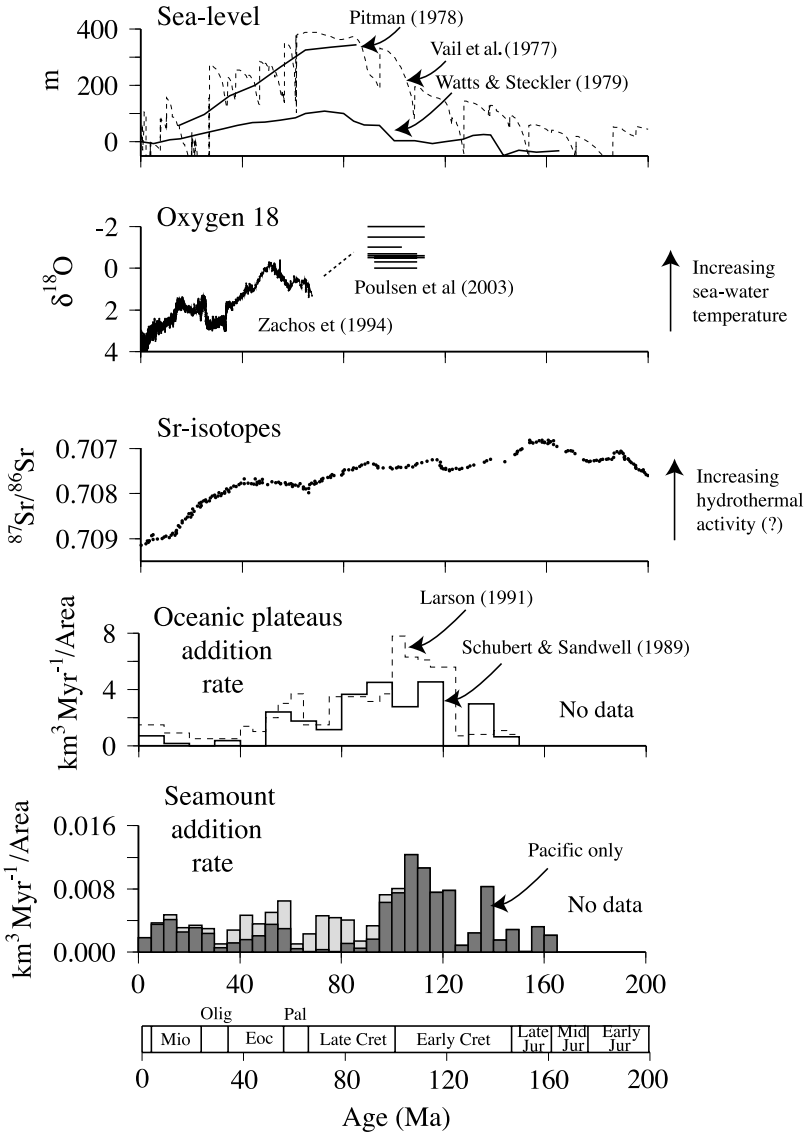

Figure 17. Global seamount and oceanic plateau addition rate through time and its relationship to changes in the seawater strontium and foraminiferal oxygen 18 isotope record and sea level. The global seamount addition rate is based on volume and age estimates at those sites where $0 < T_e < 12$ km. The oceanic plateau addition rate is based on the work by *Schubert and Sandwell* [1989] and *Larson* [1991]. Note that the *Schubert and Sandwell* [1989] rate is based on volumes of oceanic plateaus above normal seafloor depth (i.e., their V1 and V2) while the *Larson* [1991] rate is based on volumes of *Schubert and Sandwell* [1989] with the addition of the crustal root and potential symmetric twin plateaus. The strontium isotope record is based on the work by *Jones and Jenkyns* [2001], and the oxygen 18 isotope record is based on the work by *Zachos et al.* [1994] and *Poulsen et al.* [2003].

hypothesis. We show in Figure 16, for example, the T_e expected for two cases: one where the volcanism is the same age (0 Ma) along the entire length of the chain and the other where the age increases from 0 to 5 Ma and is then constant with age. In both cases, T_e increases with age because loading occurs on progressively older seafloor. Figure 16 shows, however, that neither case can account for the T_e derived from bathymetric prediction. Only the hot spot hypothesis can explain the predicted T_e. Therefore bathymetric prediction has the potential to discriminate between the two competing hypotheses, especially at seamount chains that are emplaced on young oceanic lithosphere where the change T_e is expected to be the greatest.

7.3. Addition Rate of Seamounts Through Time

[75] The *Wessel* [2001] global database includes information on the size of seamounts, banks and rises and so can be used, together with our new T_e estimates, to calculate the volume and, possibly, the rate of addition of submarine volcanism through space and time.

[76] We calculated the volume using estimates of seamount base radius and height from *Wessel* [2001] and the formula for the volume of a frustum. The total volume of

the 9758 seamounts that yielded a T_e estimate is 7.8×10^6 km^3, the largest contribution to which (71%) comes from the Pacific. This compares to the volume of 10.0×10^6 km^3 that would have been obtained if we had used all the seamounts in the database. This volume does not include any material that may infill the flexural depression or that may have underplated the flexed oceanic crust.

[77] While these volumes are significant, they are small when compared to the magmatic material that is produced at mid-ocean ridges and oceanic plateaus. The volume of oceanic crust that has been created at mid-oceanic ridges is 1448×10^6 km^3 [*Cogne and Humler*, 2004] while the volume of material that has been added to the surface and base of the oceanic crust at the oceanic plateaus is 33.1×10^6 km^3 [*Schubert and Sandwell*, 1989].

[78] Nevertheless, the rate at which seamounts have been added to the top of the oceanic crust might be significant. Figure 17 shows the addition rate as a function of time for the limited on-ridge data set and compares it to other geophysical and geochemical proxies. Figure 17 shows a general agreement between the seamount addition rate and the oceanic plateau addition rate, as computed by *Schubert and Sandwell* [1989] and *Larson* [1991]. Both rate calculations show an increase at ~120 Ma and then a decrease to the present-day. The main difference is that the seamount addition rate is higher prior to ~120 Ma than it is subsequently, while the oceanic plateau rate is less. However, this may be a result of the lack of information on past oceanic plateaus and seamounts, such as those associated with Tethys and other oceans that have long since closed.

[79] The general decrease in seamount and oceanic plateau addition rate since ~80 Ma correlates with a decrease in global sea level and, interestingly, an increase in seawater strontium and foraminiferal oxygen stable isotopes. The increase in seawater $^{87}Sr/^{86}Sr$ has been interpreted in terms of a decrease in hydrothermal activity [*Jones and Jenkyns*, 2001] while the increase in foraminiferal $\delta^{18}O$ ratios has been interpreted in terms of a decrease in sea surface water temperature [*Zachos et al.*, 2001]. These correlations suggest some link between submarine volcanism, hydrothermal activity, and sea surface water temperatures. Despite their small volumes, compared to oceanic plateaus, seamounts are important because of their wide distribution, tall pedestal heights and steep, unstable, slopes. Indeed, there is evidence that seamounts might influence such diverse phenomena as hydrothermal circulation [*Harris et al.*, 2004], mesoscale eddies [*Hogg*, 1980], and biological activity [*Rogers*, 1994]. Therefore any attempt to seek links between tectonic activity (e.g., rifting) and the history of the Earth's climate should, we believe, also take into account seamounts and their distribution through space and time.

8. Conclusions

[80] We draw the following conclusions from this study:

[81] 1. The gravity field derived from satellite altimeter data can be used to predict global bathymetry for different values of the elastic thickness of the oceanic lithosphere, T_e.

[82] 2. By comparing the predicted bathymetry to shipboard bathymetry measurements we have obtained 9758 estimates of T_e at seamounts, banks and rises in the Pacific, Indian, and Atlantic oceans.

[83] 3. Estimation of T_e at the same localities as previous studies shows that bathymetric prediction is a robust way to estimate T_e and its lower and upper bounds.

[84] 4. Estimation of T_e at 291 sites of known sample and crustal age, however, shows that there is no simple relationship between T_e and age, and no single controlling isotherm that describes all the data.

[85] 5. The average density and T_e of the 9758 estimates is 2810.6 ± 148.5 kg m^{-3} and 18.4 ± 11.0 km, respectively. We attribute the high standard deviations to the wide range rock types and tectonic settings associated with submarine volcanism.

[86] 6. The Pacific, Atlantic, and Indian oceans are characterized by a mix of tectonic settings such that seamounts that formed on ridge are in close proximity to flank ridge and off-ridge seamounts.

[87] 7. The highest concentration of on-ridge seamounts is in the south central and western Pacific. Interspersed among the on-ridge estimates are flank ridge and off-ridge estimates. Off-ridge settings dominate in the eastern North Atlantic, while flank ridge settings dominate the northwestern Indian and western South Atlantic oceans.

[88] 8. By assuming that T_e at the on-ridge estimates reflect the age of their underlying oceanic crust, we have estimated the age of >1500 seamounts.

[89] 9. The volcanism shows peaks in activity during the Early/Late Cretaceous, early Eocene, and Miocene.

[90] 10. The rate of on-ridge seamount addition appears to have decreased with time, from a peak of 0.012 km^3 yr^{-1} during the Late/Early Cretaceous to only ~0.002 km^3 yr^{-1} at the present-day. These rates are small, however, when compared to the rate of addition of oceanic plateaus (2.3 km^3 yr^{-1}) and oceanic crust at mid-ocean ridges (18.1 km^3 yr^{-1}).

[91] **Acknowledgments.** This work was completed while one of us (A.B.W.) was a Visiting Professor at the Scripps Institution of Oceanography. We thank A. Koppers, H. Staudigel, and J. Winterer for discussions on the tectonics of the Pacific Ocean basin; D. Forsyth, M. McNutt, and an anonymous reviewer for their critical comments; and the Green Scholar Programme for support. This work was also supported by a NASA (NAG5-13673) and NSF (OCE03-26707) grant to D.T.S. for retracking of the radar altimeter waveforms for gravity field improvement and a NSF grant OCE99-06773 to P.W. W.H.F.S. acknowledges NOAA. The contents of this paper, however, are solely the opinions of the authors and do not constitute a statement of policy, decision, or position on behalf of NOAA or the U.S. Government.

References

Bonatti, E., and C. G. A. Harrison (1976), Hot lines in the Earth's mantle, *Nature*, *263*, 402–404.

Bonatti, E., C. G. A. Harrison, D. E. Fisher, J. Honnerez, J.-G. Schilling, J. J. Stipp, and M. Zentilli (1977), Easter volcanic chain (southeast Pacific): A mantle hot line, *J. Geophys. Res.*, *82*, 2457–2478.

British Oceanographic Data Centre (2003), The GEBCO digital atlas, Centenary edition [CD-ROM], Liverpool, U.K.

Caldwell, J. G., and D. L. Turcotte (1979), Dependence of the elastic thickness of the oceanic lithosphere on age, *J. Geophys. Res.*, *84*, 7572–7576.

Calmant, S. (1987), The elastic thickness of the lithosphere in the Pacific Ocean, *Earth Planet. Sci. Lett.*, *85*, 277–288.

Calmant, S., and A. Cazenave (1987), Anomalous elastic thickness of the oceanic lithosphere in the south-central Pacific, *Nature*, *32*, 236–238.

Calmant, S., J. Francheteau, and A. Cazenave (1990), Elastic layer thickening with age of the oceanic lithosphere, *Geophys. J. Int.*, *100*, 59–67.

Carracedo, J. C., S. Day, H. Guillou, E. R. Rodriguez Badiola, J. A. Canas, and F. J. Perez Torrado (1998), Hotspot volcanism close to a passive continental margin: The Canary Islands, *Geol. Mag.*, *135*, 591–604.

Cazenave, A., and K. Dominh (1984), Geoid heights over the Louisville Ridge (South Pacific), *J. Geophys. Res.*, *89*, 11,171–11,179.

Charvis, P., A. Laesanpura, J. Gallart, A. Hirn, J.-C. Lepine, B. de Voogd, T. A. Minshull, Y. Hello, and B. Pontoise (1999), Spatial distribution of hotspot material added to the lithosphere under La Reunion, from wide-angle seismic data, *J. Geophys. Res.*, *104*, 2875–2893.

Clague, D. A., and G. B. Dalrymple (1987), The Hawaiian-Emperor volcanic chain. part I. Geologic evolution, in *Volcanism in Hawaii*, edited by R. W. Decker, T. L. Wright, and P. H. Stauffer, *U.S. Geol. Surv. Prof. Pap.*, *1350*, 5–54.

Clouard, V., and A. Bonneville (2001), How many Pacific hotspots are fed by deep-mantle plumes?, *Geology*, *29*, 695–698.

Clouard, V., A. Bonneville, and P.-Y. Gillot (2003), The Tarava seamounts: A newly characterized hotspot chain on the South Pacific Superswell, *Earth Planet. Sci. Lett.*, *207*, 117–130.

Cochran, J. R. (1979), An analysis of isostasy in the world's oceans: 2. Mid-ocean ridge crests, *J. Geophys. Res.*, *84*, 4713–4729.

Cogne, J.-P., and E. Humler (2004), Temporal variation of oceanic spreading and crustal production rates during the last 180 Myr, *Earth Planet. Sci. Lett.*, *227*, 427–439.

Cousens, B., J. Dostal, and T. S. Hamilton (1999), A near-ridge origin for seamounts at the southern terminus of the Pratt-Welker Seamount Chain, northeast Pacific Ocean, *Can. J. Earth Sci.*, *36*, 1021–1031.

Curry, J. R., and T. Munasinghe (1991), Origin of the Rajmahal Traps and the 85°E Ridge: Preliminary reconstructions of the trace of the Crozet hotspot, *Geology*, *19*, 1237–1240.

Davis, A. S., L. B. Gray, D. A. Clague, and J. R. Hein (2002), The Line Islands revisited: New $^{40}Ar/^{39}Ar$ geochronologic evidence for episodes of volcanism due to lithospheric extension, *Geochem. Geophys. Geosyst.*, *3*(3), 1018, doi:10.1029/2001GC000190.

Dixon, T. H., M. Naraghi, M. K. McNutt, and S. M. Smith (1983), Bathymetric prediction from Seasat altimeter data, *J. Geophys. Res.*, *88*, 1563–1571.

Duncan, R. A. (1991), Age distribution of volcanism along aseismic ridges in the eastern Indian Ocean, *Proc. Ocean Drill. Program Sci. Results*, *121*, 507–517.

Duncan, R. A., and R. B. Hargaves (1990), $^{40}Ar/^{39}Ar$ geochronology of basement rocks from the Mascarene Plateau, the Chagos bank, and the Maldives Ridge, *Proc. Ocean Drill. Program Sci. Results*, *115*, 43–51.

Epp, D. (1984), Possible perturbations to hotspot traces and implications for the origin and structure of the Line Islands, *J. Geophys. Res.*, *89*, 11,273–11,286.

Exon, N. F., M. D. Raven, and E. H. De Carlo (2002), Ferromanganese nodules and crusts from the Christmas Island region, Indian Ocean, *Mar. Georesour. Geotechnol.*, *20*, 275–297, doi:10.1080/0360886029005195.

Filmer, P. E., M. K. McNutt, and C. J. Wolfe (1993), Elastic thickness of the lithosphere in the Marquesas and Society Islands, *J. Geophys. Res.*, *98*, 19,565–19,577.

Gente, P., J. Dyment, M. Maia, and J. Goslin (2003), Interaction between the Mid-Atlantic Ridge and the Azores hot spot during the last 85 Myr: Emplacement and rifting of the hot spot-derived plateaus, *Geochem. Geophys. Geosyst.*, *4*(10), 8514, doi:10.1029/2003GC000527.

Goodwillie, A. M. (1995), Short-wavelength gravity lineations and unusual flexure results at the Puka Puka volcanic ridge system, *Earth Planet. Sci. Lett.*, *136*, 297–314.

Goodwillie, A. M., and A. B. Watts (1993), An altimetric and bathymetric study of elastic thickness in the central Pacific Ocean, *Earth. Planet. Sci. Lett.*, *118*, 311–326.

Gunn, B. M., C.-Y. Ramon, N. Watkins, C. E. Abranson, and J. Nougier (1970), Geochemistry of an oceanite-Ankaramite-Basalt suite from East Island, Crozet Archipelago, *Contrib. Mineral. Petrol.*, *28*, 319–339.

Harris, R. N., and D. S. Chapman (1994), A comparison of mechanical thickness estimates from trough and seamount loading in the southeastern Gulf of Alaska, *J. Geophys. Res.*, *99*, 9297–9317.

Harris, R. N., A. T. Fisher, and D. S. Chapman (2004), Fluid flow through seamounts and implications for global mass fluxes, *Geology*, *32*, 725–728.

Haxby, W. F., and J. K. Weissel (1986), Evidence for small-scale mantle convection from Seasat altimeter data, *J. Geophys. Res.*, *91*, 3507–3520.

Hogg, N. G. (1980), Effects of bottom topography on ocean currents, in *Orographic Effects in Planetary Flows*, *GARP Publ.*, vol. 23, edited by R. Hide and P. W. White, pp. 167–205, World Meteorol. Org., Geneva.

Jackson, E. D., and H. R. Shaw (1975), Stress fields in the Pacific plate: Delineated in time by linear volcanic chains, *J, Geophys. Res.*, *80*, 1861–1874.

Johnson, K. T. M., D. W. Graham, K. H. Rubin, K. Nicolaysen, D. S. Scheirer, D. W. Forsyth, E. T. Baker, and L. M. Douglas-Priebe (2000), Boomerang seamount: The active expression of the Amsterdam–St. Paul hotspot, Southeast Indian Ridge, *Earth Planet. Sci. Lett.*, *183*, 245–259.

Jones, C. E., and H. C. Jenkyns (2001), Seawater strontium isotopes, oceanic anoxic events, and seafloor hydrothermal activity in the Jurassic and Cretaceous, *Am. J. Sci.*, *301*, 112–149.

Kempe, D. R. C., and J.-G. Schilling (1974), Discovery Tablemount basalt: Petrology and geochemistry, *Contrib. Mineral. Petrol.*, *44*, 101–115.

Kopp, H., C. Kopp, J. Phipps Morgan, E. R. Flueh, W. Weinrebe, and W. J. Morgan (2003), Fossil hot spot-ridge interaction in the Musicians Seamount Province: Geophysical investigations of hot spot volcanism at volcanic elongated ridges, *J. Geophys. Res.*, *108*(B3), 2160, doi:10.1029/2002JB002015.

Koppers, A. A. P., and H. Staudigel (2005), Asynchronous bends in Pacific seamount trails: A case for extensional volcanism?, *Science*, *307*, 904–907.

Koppers, A. A. P., H. Staudigel, J. R. Wijbrans, and M. S. Pringle (1998), The Magellan seamount trail: Implications for Cretaceous hotspot volcanism and absolute Pacific plate motion, *Earth Planet. Sci. Lett.*, *163*, 53–68.

Koppers, A. A. P., J. Phipps Morgan, J. W. Morgan, and H. Staudigel (2001), Testing the fixed hotspot hypothesis using $^{40}Ar/^{39}Ar$ age progressions along seamount trails, *Earth Planet. Sci. Lett.*, *185*, 237–252.

Koppers, A. A. P., H. Staudigel, M. S. Pringle, and J. R. Wijbrans (2003), Short-lived and discontinuous intraplate volcanism in the South Pacific: Hot spots or extensional volcanism?, *Geochem. Geophys. Geosyst.*, *4*(10), 1089, doi:10.1029/2003GC000533.

Krishna, K. S. (1997), Isostatic response of the Central Indian Ridge (western Indian Ocean) based on transfer function analysis of gravity and bathymetry data, *Tectonophysics*, *257*, 137–148.

Krishna, K. S. (2003), Structure and evolution of the Afanasy Nikitin seamount, buried hills and 85°E Ridge in the northeastern Indian Ocean, *Earth Planet. Sci. Lett.*, *209*, 379–394.

Lago, B., and A. Cazenave (1981), State of stress in the oceanic lithosphere in response to loading, *Geophys. J. R. Astron. Soc.*, *64*, 785–799.

Larson, R. L. (1991), Latest pulse of Earth: Evidence for a mid-Cretaceous superplume, *Geology*, *19*, 547–550.

Lyons, S. N., D. T. Sandwell, and W. H. F. Smith (2000), Three-dimensional estimation of elastic thickness under the Louisville Ridge, *J. Geophys. Res.*, *105*, 13,239–13,252.

Maia, M., and J. Arkani-Hamed (2002), The support mechanism of the young Foundation Seamounts inferred from bathymetry and gravity, *Geophys. J. Int.*, *149*, 190–210.

Manea, M., V. C. Manea, V. Kostoglodov, and M. Guzman-Speziale (2005), Elastic thickness of the oceanic lithosphere beneath the Tehuantepec Ridge, *Geofis. Int.*, *44*, 157–168.

McDougall, I. (1971), The geochronology and evolution of the young oceanic island of Reunion, Indian Ocean, *Geochem. Cosmochim. Acta*, *35*, 261–270.

McDougall, I., and R. A. Duncan (1988), Age progressive volcanism in the Tasmantid Seamounts, *Earth Planet. Sci. Lett.*, *89*, 207–220.

McKenzie, D. P., and C. O. Bowin (1976), The relationship between bathymetry and gravity in the Atlantic Ocean, *J. Geophys. Res.*, *81*, 1903–1915.

McNutt, M. K. (1979), Compensation of oceanic topography: An application of the response function technique to the Surveyor area, *J. Geophys. Res.*, *84*, 7589–7598.

McNutt, M. K., and H. W. Menard (1978), Lithospheric flexure and uplifted atolls, *J. Geophys. Res.*, *83*, 1206–1212.

McNutt, M., D. Caress, J. Reynolds, K. A. Jordahl, and R. A. Duncan (1997), Failure of plume theory to explain midplate volcanism in the southern Austral Islands, *Nature*, *389*, 479–482.

Menard, H. W. (1964), *Marine Geology of the Pacific*, 271 pp., McGraw-Hill, New York.

Moreira, M., T. Staudacher, P. Sarda, J. G. Schilling, and C. J. Allegre (1995), A primitive plume neon component in MORB: The Shona ridge-anomaly, South Atlantic (51–52°S), *Earth Planet. Sci. Lett.*, *133*, 367–377.

Müeller, R. D., W. R. Roest, J.-Y. Royer, L. M. Gahagan, and J. G. Sclater (1997), Digital isochrons of the world's ocean floor, *J. Geophys. Res.*, *102*, 3211–3214.

Natland, J. H., and E. L. Winterer (2005), Fissure control on volcanic action in the Pacific, in *Plumes, Plates and Paradigms*, edited by G. R. Foulger et al., *Spec. Pap. Geol. Soc. Am.*, *388*, 687–710.

Nettleton, L. L. (1939), Determination of density for reduction of gravity observations, *Geophysics*, *4*, 176–183.

O'Connor, J. M., and R. A. Duncan (1990), Evolution of the Walvis Ridge–Rio Grande Rise hot spot system: Implications for African and South American plate motions over plumes, *J. Geophys. Res.*, *95*, 17,475–17,502.

O'Connor, J. M., P. Stoffers, and J. R. Wijbrans (1998), Migration rate of volcanism along the Foundation Chain, SE Pacific, *Earth Planet. Sci. Lett.*, *164*, 41–59.

O'Connor, J. M., P. Stoffers, P. van den Bogaard, and M. McWilliams (1999), First seamount age evidence for significantly slower African plate motion since 19 to 30 Ma, *Earth Planet. Sci. Lett.*, *171*, 575–589.

O'Connor, J. M., P. Stoffers, and J. R. Wijbrans (2002), Pulsing of a focused mantle plume: Evidence from the distribution of foundation chain hotspot volcanism, *Geophys. Res. Lett.*, *29*(9), 1350, doi:10.1029/2002GL014681.

Parker, R. L. (1972), The rapid calculation of potential anomalies, *Geophys. J. R. Astron. Soc.*, *31*, 447–455.

Parsons, B. (1982), Causes and consequences of the relation between area and age of the ocean floor, *J. Geophys. Res.*, *87*, 289–302.

Parsons, B., and J. G. Sclater (1977), Ocean floor bathymetry and heat flow, *J. Geophys. Res.*, *82*, 803–827.

Patriat, M., F. Klingelhoefer, D. Aslanian, I. Contrucci, M. Gutscher, J. Talandier, F. Avedik, J. Francheteau, and W. Weigel (2002), Deep crustal structure of the Tuamotu plateau and Tahiti (French Polynesia) based on seismic refraction data, *Geophys. Res. Lett.*, *29*(14), 1656, doi:10.1029/2001GL013913.

Pitman, W. C. (1978), The relationship between eustasy and stratigraphic sequences of passive margins, *Geol. Soc. Am. Bull.*, *89*, 1389–1403.

Poulsen, C. J., A. S. Gendaszek, and R. L. Jacob (2003), Did the rifting of the Atlantic Ocean cause the Cretaceous thermal maximum?, *Geology*, *31*, 115–118.

Ramillien, G., and P. Mazzega (1999), Non-linear altimetric geoid inversion for lithospheric elastic thickness and crustal density, *Geophys. J. Int.*, *138*, 667–678.

Ribe, N. M. (1982), On the interpretation of frequency response functions for oceanic gravity and bathymetry, *Geophys. J. R. Astron. Soc.*, *70*, 273–827.

Rogers, A. D. (1994), The biology of seamounts, *Adv. Mar. Biol.*, *30*, 305–350.

Sager, W. W., and H.-C. Han (1993), Rapid formation of the Shatsky Rise oceanic plateau inferred from its magnetic anomaly, *Nature*, *364*, 610–613.

Sandwell, D. T., and W. H. F. Smith (1997), Marine gravity anomaly from Geosat and ERS-1 satellite altimetry, *J. Geophys. Res.*, *102*, 10,039–10,054.

Sandwell, D. T., E. L. Winterer, J. Mammerickx, R. A. Duncan, M. A. Lynch, D. A. Levitt, and C. L. Johnson (1995), Evidence for diffuse extension of the Pacific plate from Pukapuka ridges and cross-grain gravity lineations, *J. Geophys. Res.*, *100*, 15,087–15,099.

Schlanger, S. O., M. Garcia, B. H. Keating, J. J. Naughton, W. W. Sager, J. A. Haggerty, J. A. Philpott, and R. A. Duncan (1984), Geology and geochronology of the Line Islands, *J, Geophys. Res.*, *89*, 11,261–11,272.

Schubert, J., and D. T. Sandwell (1989), Crustal volumes of the continents and of oceanic and continental submarine plateaus, *Earth Planet. Sci. Lett.*, *92*, 234–246.

Searle, R. C., J. Francheteau, and B. Cornaglia (1995), New observations on mid-plate volcanism and the tectonic history of the Pacific plate, Tahiti to Easter microplate, *Earth Planet. Sci. Lett.*, *131*, 395–421.

Smith, W. H. F., and D. T. Sandwell (1994a), Bathymetric prediction from dense satellite altimetry and sparse shipboard bathymetry, *J. Geophys. Res.*, *99*, 21,803–21,824.

Smith, W. H. F., and D. T. Sandwell (1994b), Elastic lithosphere thickness estimated from dense satellite altimetry and sparse shipboard bathymetry, *Eos Trans. AGU*, *75*, 154.

Smith, W. H. F., and D. T. Sandwell (1997), Global sea floor topography from satellite altimetry and ship depth soundings, *Science*, *277*, 1956–1962.

Smith, W. H. F., H. Staudigel, A. B. Watts, and M. S. Pringle (1989), The Magellan Seamounts: Early Cretaceous record of the South Pacific isotopic and thermal anomaly, *J. Geophys. Res.*, *94*, 10,501–10,523.

Staudigel, H., K. H. Park, M. S. Pringle, J. L. Rubenstone, W. H. F. Smith, and A. Zindler (1991), The longevity of the South Pacific isotopic and thermal anomaly, *Earth Planet. Sci. Lett.*, *102*, 24–44.

Stillman, C. J., H. Furnes, M. J. Le Bas, A. H. F. Robertson, and J. Zielonka (1982), The geological history of Maio, Cape Verde Islands, *J. Geol. Soc. London*, *139*, 347–361.

Vail, P. R., R. M. Mitchum, and S. Thompson (1977), Relative sea–level from coastal onlap, in *Seismic Stratigraphy: Applications to Hydrocarbon Exploration*, edited by C. E. Payton, *AAPG Mem.*, *26*, 63–82.

Verhoef, J. (1984), A geophysical study of the Atlantis-Meteor seamount complex, Ph.D. thesis, Univ. of Utrecht, Utrecht.

Watts, A. B. (1978), An analysis of isostasy in the world's oceans: 1, Hawaiian-Emperor Seamount Chain, *J. Geophys. Res.*, *83*, 5989–6004.

Watts, A. B. (1983), The strength of the Earth's crust, *J. Mar. Technol.*, *17*, 12.

Watts, A. B. (2001), *Isostasy and Flexure of the Lithosphere*, 458 pp., Cambridge Univ. Press, New York.

Watts, A. B., and M. S. Steckler (1979), Subsidence and eustasy at the continental margin of eastern North America, in *Deep Drilling Results in the Atlantic Ocean: Continental Margins and Paleoenvironment*, *Maurice Ewing Ser.*, vol. 3, edited by M. Talwani, et al, pp. 218–234, AGU, Washington, D. C.

Watts, A. B., and U. S. ten Brink (1989), Crustal structure, flexure and subsidence history of the Hawaiian Islands, *J. Geophys. Res.*, *94*, 10,473–10,500.

Watts, A. B., and S. Zhong (2000), Observations of flexure and the rheology of oceanic lithosphere, *Geophys. J. Int.*, *142*, 855–875.

Watts, A. B., J. R. Cochran, and G. Selzer (1975), Gravity anomalies and flexure of the lithosphere: A three-dimensional study of the Great Meteor Seamount, N.E. Atlantic, *J. Geophys. Res.*, *80*, 1391–1398.

Watts, A. B., J. H. Bodine, and N. M. Ribe (1980), Observations of flexure and the geological evolution of the Pacific Ocean basin, *Nature*, *283*, 532–537.

Watts, A. B., J. R. Cochran, P. Patriat, and M. Doucoure (1985), A bathymetry and altimetry profile of the Southwest Indian Ridge at 31°S, *Earth Planet. Sci. Lett.*, *73*, 129–139.

Watts, A. B., J. K. Weissel, R. A. Duncan, and R. L. Larson (1988), Origin of the Louisville Ridge and its relationship to the Eltanin Fracture Zone system, *J. Geophys. Res.*, *93*, 3051–3077.

Wessel, P. (1992), Thermal stresses and the bimodal distribution of elastic thickness estimates of the oceanic lithosphere, *J. Geophys. Res.*, *97*, 14,177–14,193.

Wessel, P. (1997), Sizes and ages of seamounts using remote sensing: Implications for intraplate volcanism, *Science*, *277*, 802–805.

Wessel, P. (2001), Global distribution of seamounts inferred from gridded Geosat/ERS-1 altimetry, *J. Geophys. Res.*, *106*, 19,431–19,442.

White, W. M., and R. A. Duncan (1996), Geochemistry and geochronology of the Society Islands: New evidence for deep mantle recycling, in *Earth Processes: Reading the Isotopic Code*, *Geophys. Monogr. Ser.*, vol. 95, edited by A. Basu and S. Hart, pp. 183–206, AGU, Washington, D. C.

Woodroffe, C. D. (1988), Vertical movement of isolated oceanic islands at plate margins: Evidence from emergent reefs in Tonga (Pacific Ocean) Cayman Islands (Caribbean Sea) and Christmas Island (Indian Ocean), *Z. Geomorphol.*, *Suppl. 69*, 17–37.

Zachos, J. C., L. D. Scott, and K. C. Lohmann (1994), Evolution of early Cenozoic marine temperatures, *Paleooceanography*, *9*, 353–387.

Zachos, J., M. Pagani, L. Sloan, E. Thomas, and K. Billups (2001), Trends, rhythms, and aberrations in global climate, 65 Ma to present, *Science*, *292*, 686–693.

Zheng, Y., and J. Arkani-Hamed (2002), Rigidity of the Atlantic oceanic lithosphere beneath New England seamounts, *Tectonophysics*, *359*, 359–369.

D. T. Sandwell, Scripps Institution of Oceanography, MC 0225, University of California, San Diego, La Jolla, CA 92093-0225, USA.

W. H. F. Smith, Laboratory for Satellite Altimetry, NOAA, MC E/RA31, 1335 East-West Highway, Room 5408, Silver Spring, MD 20910-3282, USA.

A. B. Watts, Department of Earth Sciences, University of Oxford, Parks Road, Oxford OX1 3PR, UK. (tony@earth.ox.ac.uk)

P. Wessel, Department of Geology and Geophysics, SOEST, University of Hawaii, 1680 East-West Road, Honolulu, HI 96822, USA.